Hamiltonian formulation of water waves

1D-formulation, numerical evaluations and examples

A.K. Otta and M.W. Dingemans

May 1994

Executive's summary

This report describes the formulation, numerical implementation and application of a weakly nonlinear wave model for finite depth based on a Hamiltonian formulation (see Radder, 1992). Due to the type of nonlinearity explicitly accounted for in the expansion of the kernel of the Hamiltonian density (sum of kinetic and potential energy per unit surface area), the model is valid for waves of small, but finite amplitude and fairly long wave length (compared to the water depth) in roughly the same sense many 'Boussinesq-type' models are. There are, however, a few significant differences. Firstly, the Hamiltonian density in the present formulation is always *positive definite*: a condition necessary to ensure good dynamical behaviour of the model equations for numerical computation. Secondly, the dispersion equation obtained from the linearised version of the equations is exact. This property results in a better modelling of the phase relations (hence the wave asymmetry at a given location) of the superharmonic field which evolves from the primary wave system due to surface nonlinearity. More importantly, it is possible to remove the restriction of waves being long through a proper inclusion of the 'short-wave' nonlinearity in the expansion of the kernel. This results in a uniformly valid model unlike most of the weakly nonlinear models which are valid over either deep or shallow water. Further, it is discussed in the text that even for long waves the 'short-wave' nonlinearity becomes locally important near the crest of a wave as the surface curvature increases. Implementation of 'short-wave' nonlinearity is therefore considered as one of the first priorities in the future developments of the model.

Two numerical models have been developed: a time-domain model and a pseudo-spectral model based on the sinc-series for the global approximations. The numerical code based on the sinc-series requires less computing time and gives the option of choosing higher-order interpolation for computing derivatives and integrals over local intervals. We present here a figure as an example of the model prediction of nonlinear evolution of a train of non-breaking waves passing over an underwater bar. An incident train of sinusoidal waves has been represented in the computation by a packet of sinusoidal waves of finite length with the leading edge a few wave-lengths behind the bar. Details of the geometry and significance of this test can be found in chapter 7. In

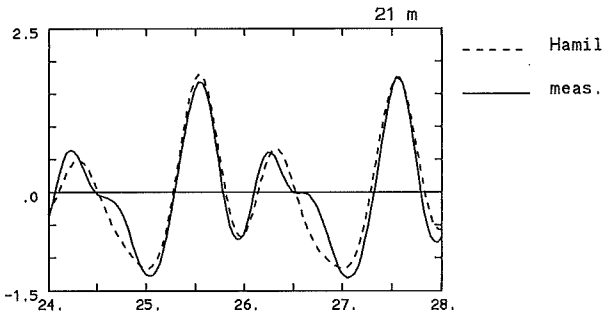

spite of a practical disadvantage due to the way the input conditions must be specified in the code (we have an initial-value problem) these models can now be used to study nonlinear evolutions of nonbreaking waves over varying depth.

Attempts to introduce effects of wave breaking have not met with much success yet. In

the first phase, an integral criterion has been implemented to determine if the instantaneous surface shape should lead to breaking. Application of the criterion to computed surface elevation for conditions observed to have given rise to mild breaking in laboratory tests shows that breaking stage is not reached. It is believed that this difference between the computed results and the laboratory observations is caused by the omission of the 'short-wave' nonlinearity (underprediction of the surface steepness), rather than the failure of the integral criterion. This is another aspect which underscores the importance of implementation of 'short-wave' nonlinearity.

Finally to conclude, comparison of the computed results with the experimental measurements and in a wider context with several 'Boussinesq-type' models (see Dingemans, 1994a) provides strong motivation for further developments of the model. This is further supported by the inherent theoretical appeal of the formulations used. As summarised in chapter 9, the major recommendations for future work are:

- The formulation of a boundary-value problem instead of an initial-value problem. This greatly enhances the practical usefulness of the program.
- Inclusion of short-wave nonlinearity. For applicability over the full range of deep to shallow water of a nonlinear wave model, inclusion of short-wave nonlinearity is needed. Furthermore, it has been shown that for wave breaking also the inclusion of short-wave nonlinearity is needed to obtain more realistic breaker indices.
- Further study of wave breaking characteristics after inclusion of short-wave nonlinearity.
- Effect of steeper bottom slopes on the wave behaviour.

Contents

1 Introduction

In this report the study into the properties and numerical behaviour of the equations proposed by Radder (1992) is described.

At first, in Chapter 2, the mathematical formulation is given. This follows closely Radder (1992). It is important to note that the present treatment is strictly valid only for 1D wave propagation. This is due to the fact that the methods rest upon conformal transformations. Furthermore, in course of the derivation, use is made of the assumption that the variation of the still-water depth is absent in the Hamiltonian. This may be compared with the way in which the mild-slope equation is derived: for the classical mild-slope equation no variation of the depth is included in the Hamiltonian, but for the extended equation variations of the depth in the Hamiltonian have to be included, see Dingemans (1994b, Chapter 3).

The numerical evaluation of the evolution equations for the time-domain model is described in chapter 3.

A spectral approach based on an expansion in terms of sinc functions is described in chapter 4. The basic idea behind such a spectral description is to obtain improved numerical efficiency. The time-domain model still takes much computer time, especially because the evaluation of the kernel log tanh() which has to be evaluated over the whole computational domain. Earlier attempts to terminate the computation of this kernel beyond a local interval to take advantage of the rapid decay of the kernel had no success. Instabilities developed then very soon from near the ends of the geometry. It should be emphasised that spectral solution based on the Fourier-series expansion over a finite span has been found to be unsuccessful for the present Hamiltonian formulation. Three possible approaches based on sinc series have been discussed in chapter 4. The numerical procedure for one of the three approaches has been described in chapter 5.

A short description of the programs is given in chapter 6. Some numerical examples have been given in chapter 7.

An approach to modelling wave breaking has been discussed in chapter 8, followed by the conclusions in chapter 9.

The research has been carried out by A.K. Otta and M.W. Dingemans, while the constant guidance of A.C. Radder of Rijkswaterstaat has been invaluable.

2 The mathematical model

2.1 The Hamiltonian formulation

The governing equations for irrotational wave motion on an incompressible inviscid fluid are given by the Laplace equation and the three boundary conditions:

$$\nabla^2\Phi + \frac{\partial^2\Phi}{\partial z^2} = 0 \quad ; \quad -h(\boldsymbol{x}) \le z \le \zeta(\boldsymbol{x},t) \tag{2.1a}$$

$$\frac{\partial\Phi}{\partial t} + \frac{1}{2}\left\{(\nabla\Phi)^2 + \left(\frac{\partial\Phi}{\partial z}\right)^2\right\} - \mathsf{T}[\zeta] + g\zeta = 0 \quad ; \quad z = \zeta(\boldsymbol{x},t) \tag{2.1b}$$

$$\frac{\partial\zeta}{\partial t} + \nabla\Phi\cdot\nabla\zeta = \frac{\partial\Phi}{\partial z} \quad ; \quad z = \zeta(\boldsymbol{x},t) \tag{2.1c}$$

$$\frac{\partial\Phi}{\partial z} + \nabla\Phi\cdot\nabla h = 0 \quad ; \quad z = -h(\boldsymbol{x}), \tag{2.1d}$$

where

$$\mathsf{T}[\zeta] = \gamma\,\nabla\cdot\left[\frac{\nabla\zeta}{\left(1+|\nabla\zeta|^2\right)^{1/2}}\right], \tag{2.1e}$$

and γ is the surface tension and two-dimensional vectors have been used, $\boldsymbol{x} = (x,y)^T$. It has been shown that the Hamiltonian constitutes a variational principle when it is expressed in terms of the free surface elevation ζ and the value of the velocity potential at the free surface $\varphi(\boldsymbol{x},t) = \Phi\{(\boldsymbol{x},\zeta(\boldsymbol{x},t),t\}$, see, *e.g.*, Zakharov (1968) and Broer (1974). The total energy of the fluid is given by

$$\begin{aligned}\mathcal{H} &= \iint dx\,dy\,H = \iint dx\,dy\,(V+T) = \\ &= \rho\iint dx\,dy\left\{\frac{1}{2}g\zeta^2 + \gamma\left[\sqrt{1+|\nabla\zeta|^2}-1\right]\right. \\ &\qquad \left. + \int_{-h}^{\zeta} dz\frac{1}{2}\left[(\nabla\Phi)^2 + \left(\frac{\partial\Phi}{\partial z}\right)^2\right]\right\}.\end{aligned} \tag{2.2}$$

In the sequel of this report no effect of surface tension is accounted for, i.e., $\mathsf{T} = 0$ is taken. Then we have

$$V = \frac{1}{2}\rho g\zeta^2 \quad \text{and} \quad T = \frac{1}{2}\rho\int_{-h}^{\zeta} dz\left[(\nabla\Phi)^2 + \left(\frac{\partial\Phi}{\partial z}\right)^2\right]. \tag{2.3}$$

The variation of the Hamiltonian, given by (2.2), is equivalent with the original full set of water wave equations. However, one has the opportunity to find approximate equations from an approximation of the Hamiltonian with the advantage that good dynam-

ical behaviour is guaranteed when the positive definiteness of the exact Hamiltonian density H is also carried over to the approximate density H_a. Every approximation $\mathcal{H}_a$ which maintains the symmetries of $\mathcal{H}$ guarantees automatically the corresponding conservation laws to hold.

Notice that the Hamiltonian density is effectively a function of the free surface variables ζ and φ. Variation of $\mathcal{H}$ to ζ and φ gives the two canonical equations:

$$\frac{\delta \mathcal{H}}{\delta \varphi} = \rho \frac{\partial \zeta}{\partial t} \qquad \text{and} \qquad \frac{\delta \mathcal{H}}{\delta \zeta} = -\rho \frac{\partial \varphi}{\partial t} \,, \tag{2.4}$$

where δ denotes the variational derivative. Notice that Eqs. (2.4) are the free surface conditions (2.1b) and (2.1c) while Eqs. (2.1a) and (2.1d) have been used as side conditions. The major difficulty in applying the Hamiltonian is that the kinetic energy density should be formulated in terms of the surface elevation ζ and the velocity potential φ along the free surface.

In the sequel we will use a Hamiltonian which is scaled with the density: $\mathcal{H} := \mathcal{H}/\rho$ and similarly scaled potential and kinetic energy ($\mathcal{V}$ and $\mathcal{T}$ respectively) to comply with the notation used in Radder (1992).

2.2 1D-formulation

For problems with one horizontal dimension an approximate Hamiltonian can be developed which is uniformly valid from deep to shallow water (Radder, 1992). In this case, the kinetic energy density T can be written as

$$T = -\frac{1}{2}\varphi \frac{\partial \psi}{\partial x} \cong \frac{1}{2}\frac{\partial \varphi}{\partial x}\psi \,, \tag{2.5}$$

where $\psi = \Psi\{x, \zeta(x,t), t\}$ is the stream function evaluated at the free surface.

To express ψ in terms of the canonical variables φ and ζ, a conformal mapping of the fluid domain $Z = x + iz$ into an infinite strip in the complex $W-$plane $W = \chi + i\xi$ is used (Woods, 1961)

$$Z(W) = \frac{1}{2}\int_{-\infty}^{\infty} d\chi' \left\{ \tanh\left[\frac{\pi}{2}(W-\chi')\right]\zeta(\chi') + \coth\left[\frac{\pi}{2}(W-\chi')\right]h(\chi') \right\}. \tag{2.6}$$

A solution for the stream function $\Psi(x,z,t)$ at the free surface is sought for in two steps:

1. Solve the problem in the $W-$plane
2. Find the inverse transformation $\chi(x)$ along the free surface.

2.2.1 Solution in the $W-$plane

A solution of the linear problem $\frac{\partial^2\Psi}{\partial\chi^2} + \frac{\partial^2\Psi}{\partial\xi^2} = 0$ in $0 \leq \xi \leq 1$ and the boundary conditions $\Psi = 0$ at $\xi = 0$ and $\Psi = \psi(\chi)$ at $\xi = 1$ by means of Fourier transforms gives at the free surface $\xi = 1$

$$\psi(\chi) = -\frac{1}{\pi}\int_{-\infty}^{\infty}\frac{d\varphi}{d\chi'}\log\tanh\left(\frac{\pi}{4}|\chi-\chi'|\right)d\chi' \,. \tag{2.7}$$

where log is the natural logarithm. In the transformed plane the Hamiltonian $\mathcal{H}$ becomes

$$\mathcal{H} = \frac{1}{2}\int d\chi\left(g\zeta^2\frac{dx}{d\chi} + \frac{d\varphi}{d\chi}\psi(\chi)\right) \tag{2.8}$$

and with $\psi(\chi)$ substituted from (2.7) one obtains

$$\mathcal{H} = \frac{1}{2}\int d\chi\left(g\zeta^2\frac{dx}{d\chi} + \frac{\partial\varphi}{\partial\chi}\int d\chi'\frac{\partial\varphi}{\partial\chi'}\mathcal{R}(\chi,\chi')\right) \tag{2.9}$$

with the kernel $\mathcal{R}(\chi,\chi')$ given by

$$\mathcal{R}(\chi,\chi') = -\frac{1}{\pi}\log\tanh\left(\frac{\pi}{4}|\chi-\chi'|\right) \,. \tag{2.10}$$

2.2.2 The inverse transformation

To express (2.7) in terms of variables of the physical plane, an expression for the function $\chi(x)$ along the free surface has to be found. The imaginary part of the transformation (2.6) reads

$$\begin{aligned} z(\chi,\xi) \;=\; & \frac{1}{2}\int_{-\infty}^{\infty}\frac{\sin\pi\xi}{\cosh\pi\,(\chi-\chi') + \cos\pi\xi}\zeta(\chi')\,d\chi' \\ & -\frac{1}{2}\int_{-\infty}^{\infty}\frac{\sin\pi\xi}{\cosh\pi\,(\chi-\chi') - \cos\pi\xi}\,h(\chi')\,d\chi' \end{aligned} \tag{2.11}$$

Through a Fourier transform of this imaginary part a symbolic operator equation is obtained (Radder, 1992, Eq. (26)):

$$x(\chi) = \left(\frac{1}{\tan\left(\frac{d}{d\chi}\right)}\right)\zeta(\chi) + \left(\frac{1}{\sin\left(\frac{d}{d\chi}\right)}\right)h(\chi) \,. \tag{2.12}$$

This equation has to be inverted to obtain the required function $\chi(x)$. The subsequent analysis presented by Radder is valid in the strict sense for the simplified case of a horizontal bottom for which (2.12) simplifies to

$$\frac{dx}{d\chi} = \frac{d}{d\chi}\left(\cot\left(\frac{d}{d\chi}\right)\right)\eta(\chi) \tag{2.13a}$$

where the notation

$$\eta(x) = h + \zeta(x) \tag{2.13b}$$

is used.

An unknown function $\varepsilon(x)$ is introduced through

$$\frac{dx}{d\chi} = (1+\varepsilon)\,\eta\,. \tag{2.14}$$

Notice that this relation at this stage is merely another way of writing relation (2.13a).

The kinetic energy $\mathcal{T}$ can be rewritten in terms of the physical variables in the following way. First notice that

$$d\chi \to dx\frac{d\chi}{dx} \quad \text{and} \quad \frac{\partial\varphi}{\partial\chi} \to \frac{\partial\varphi}{\partial x}\frac{dx}{d\chi}\,,$$

so that

$$\frac{1}{2}\frac{\partial\varphi}{\partial\chi}\int d\chi'\,\frac{\partial\varphi}{\partial\chi'}\mathcal{R}(\chi,\chi') \to \frac{1}{2}\varphi_x\frac{dx}{d\chi}\int dx'\,\frac{d\chi'}{dx'}\varphi_{x'}\frac{dx'}{d\chi'}R(x,x')$$

$$\Rightarrow \mathcal{T} = \frac{1}{2}\int dx\,\varphi_x\int dx'\varphi_{x'}R(x,x')\,.$$

Introducing the kinetic energy density by

$$T = \frac{1}{2}\int dx'\varphi_x\varphi_{x'}\mathcal{R}_\varepsilon(x,x')\,, \tag{2.15}$$

we then have $\mathcal{T} = \int dx\,T$. The kernel $\mathcal{R}_\varepsilon$ now follows from (2.10) by noting that (2.14) gives

$$d\chi = \frac{dx}{(1+\varepsilon)\,\eta} \quad \Rightarrow \quad \chi = \int^x \frac{dr}{(1+\varepsilon)\,\eta} \quad \Rightarrow \quad |\chi-\chi'| = \left|\int_x^{x'}\frac{dr}{(1+\varepsilon)\,\eta}\right|.$$

We then have the symmetric function $\mathcal{R}_\varepsilon$ given by:

$$\mathcal{R}_\varepsilon(x,x';\eta) \equiv -\frac{1}{\pi}\log\tanh\left(\frac{\pi}{4}\left|\int_x^{x'}\frac{dr}{(1+\varepsilon)\,\eta}\right|\right)\,. \tag{2.16}$$

It is noted that the kinetic energy functional, expressed in the χ-variable, is *positive definite*, and this property is preserved on transforming from χ to x when the Jacobian (2.13a) is positive and bounded.

The Hamiltonian in the physical plane then is

$$\mathcal{H} = \frac{1}{2}\int_{-\infty}^{\infty} dx \left(g\zeta^2 + \int_{-\infty}^{\infty} dx' \varphi_x \varphi_{x'} \mathcal{R}_\varepsilon(x, x'; \eta) \right) . \tag{2.17}$$

Either to be able to use (2.17) directly to obtain evolution equations from, or to transform results obtained in the χ plane to the physical plane, it is necessary to find a prescription for the unknown function $\varepsilon(x)$. This is the subject of next subsection.

2.2.3 Non-linear integral equation

We now seek an explicit expression for the function $\varepsilon(x)$. We first notice that equation (2.13a) can be written in the form of a nonlinear integral equation (Radder, 1992) as

$$\frac{dx}{d\chi} = \eta(\chi) - \frac{1}{4}\pi \int_{-\infty}^{\infty} \frac{\eta(\chi - \chi') - \eta(\chi)}{\sinh^2 \frac{1}{2}\pi\chi'} d\chi' . \tag{2.18}$$

To solve this nonlinear integral equation, an expansion in partial fractions, which is valid for all values of the argument, is used by Radder (1992):

$$\frac{dx}{d\chi} = \eta + \sum_{m=1}^{\infty} \frac{d}{d\chi} \left[\frac{1}{\frac{d}{d\chi} - m\pi} + \frac{1}{\frac{d}{d\chi} + m\pi} \right] \eta . \tag{2.19}$$

With the notation

$$p \equiv \int_0^x \frac{dr}{\eta} \quad , \quad D \equiv \frac{d}{dp} = \eta \frac{d}{dx} , \tag{2.20}$$

and the function $\varepsilon(x)$ defined according to (2.14), an equation for ε is obtained from the expansion (2.19) as

$$\varepsilon = \frac{1}{\eta}(1+\varepsilon) \sum_{m=1}^{\infty} D \left[\frac{1}{(1+\varepsilon)D - m\pi} + \frac{1}{(1+\varepsilon)D + m\pi} \right] \eta . \tag{2.21}$$

To solve this equation for $\varepsilon(x)$, Radder introduces the operators $G_\varepsilon^{(m)}$ and $G_0^{(m)}$ by

$$G_\varepsilon^{(m)} \equiv \frac{D}{(1+\varepsilon)D - m\pi} \quad \text{and} \quad G_0^{(m)} \equiv \frac{D}{D - m\pi} , \tag{2.22}$$

and because $G_\varepsilon^{(m)}$ can be expressed iteratively in terms of $G_0^{(m)}$ we have

$$G_\varepsilon^{(m)} = \sum_{\lambda=0}^{\infty} (-1)^\lambda G_0^{(m)} \left(\varepsilon G_0^{(m)} \right)^\lambda . \tag{2.23}$$

For the function $\varepsilon(x)$ we then obtain the equation

$$\varepsilon = (1+\varepsilon)\sum_{\lambda=0}^{\infty}(-1)^{\lambda} I_{\lambda} \,, \tag{2.24a}$$

with

$$I_{\lambda} = \frac{1}{\eta}\sum_{m=1}^{\infty}\left[G_0^{(m)}\left(\varepsilon G_0^{m)}\right)^{\lambda} + G_0^{(-m)}\left(\varepsilon G_0^{(-m)}\right)^{\lambda}\right]\eta \,. \tag{2.24b}$$

Equation (2.21) or (2.24a) can now be solved iteratively as

$$\varepsilon_0 = 0 \quad , \quad \varepsilon_1 = \frac{I_0}{1-I_0} \quad , \quad \varepsilon_2 = \frac{I_0 - I_1}{1 - I_0 + I_1} \quad , \quad \cdots \tag{2.25}$$

where I_0 is given to be (see Radder, 1992)

$$I_0 = -\frac{1}{\eta(p)}\int_0^{\infty}\frac{dq}{\exp(\pi q)-1}\frac{d}{dq}\left[\eta(p+q)+\eta(p-q)\right] \,, \tag{2.26}$$

and I_1 follows as

$$\begin{aligned} I_1 \;=\; & \frac{1}{\eta(p)}\int_0^{\infty}\int_0^{\infty}\frac{dqdq'}{\exp\pi\,(q+q')-1} \\ & \times\frac{d}{dq}\left[\varepsilon_1\,(p+q)\,\frac{d}{dq'}\eta(p+q+q') + \varepsilon_1\,(p-q)\,\frac{d}{dq'}\eta(p-q-q')\right] . \end{aligned} \tag{2.27}$$

Solution for ε_k, $k = 0, 1, 2, \cdots$ can in principle be obtained through a recurring procedure in this way.

Finite depth

For water of finite depth we have[1] $\|D\| < \pi$ and a Taylor series expansion of $G_0^{(m)}$ may be used (Radder, 1992, Eq. (43)):

$$G_0^{(m)} = -\frac{D}{m\pi}\left[1 + \frac{D}{m\pi} + \left(\frac{D}{m\pi}\right)^2 + \left(\frac{D}{m\pi}\right)^3 + \cdots\right] \,, \tag{2.28}$$

and likewise for $G_0^{(-m)}$. The expansion of (2.24a) may then be given in a more convenient form. The following quantities are introduced:

$$F_k = \frac{1}{\eta}D^k\eta \,; \quad F_0 = 1 \,. \tag{2.29}$$

The following recurrence relations may then be derived from (2.29) and (2.20):

$$F\,(\eta F_k) = \eta F_{k+1} \quad \text{and} \quad DF_k = F_{k+1} - F_k F_1 \,. \tag{2.30}$$

[1] A bounded operator $\mathcal{P}$ is defined by $(f, \mathcal{P}) \leq (f, f)$ with f some well-behaved function and $(\cdot,\cdot)$ an inner product. The *norm* of the operator, $\|\mathcal{P}\|$ is defined as the maximum of $(\mathcal{P}f, \mathcal{P}f)\,/(f, f)$.

Substitution of the series expansion (2.28) in (2.23) and using the recurrence relations (2.30) then leads to an expansion of ε in terms of the functions F_k. Up to fourth order Radder obtains (his equation (46)):

$$\varepsilon = -\frac{1}{3}F_2 - \frac{1}{45}\left(F_4 - 5F_3F_1 - 10F_2^2 + 5F_2F_1^2\right) - \cdots , \tag{2.31}$$

which can be rewritten as[2] (cf. Radder, 1992, Eq. (B6))

$$\begin{aligned}\varepsilon(x,t) \;=\; & -\frac{1}{3}\left(\eta_x^2 + \eta\eta_{xx}\right) + \\ & -\frac{1}{45}\left(-9\eta_x^4 - 6\left(4\eta_x^2 + \eta\eta_x\right)\eta\eta_{xx} + 2\eta^2\eta_{xx}\eta_{xxx} + \eta^3\eta_{4x}\right) - \cdots .\end{aligned} \tag{2.32}$$

It is important to note that crucial for this approximation is the validity of the expansion (2.28). In the first place the expansion is only valid for water of finite-depth, and in the second place the expansion is a Taylor-type expansion, not yielding positive-definite approximations for the class of square integrable functions with $\eta > 0$. Perhaps a better approximation can be obtained by using a Padé -type approximation for the functions $G_0^{(m)}$.

With the Hamiltonian given by (2.17), the evolution equations for the canonical variables ζ and φ are in principle given by the defining equations (2.4). However, due to the complicated dependence on ε, derivation of the evolution equations is not a trivial task, except for the case of $\varepsilon = 0$.

2.2.4 Limiting cases

Consider the expression (2.16) for $\mathcal{R}_\varepsilon$. For a constant depth of h, we can write

$$\mathcal{R}_\varepsilon(x,x';\eta) = -\frac{1}{\pi}\log\tanh\left(\frac{\pi}{4}\left|\frac{1}{h}\int_x^{x'}\frac{dr}{(1+\varepsilon)(1+\zeta/h)}\right|\right) . \tag{2.33}$$

Linear theory is obtained for $\varepsilon = 0$ and $\eta = h$ (*i.e.*, infinitesimal waves, and thus ζ is neglected); the expression for $R_\varepsilon \equiv R_\ell$ then coincides with the one given by Broer (1974) for linear waves. For deep water it turns out that $\varepsilon = O(ka)$ and then Stokes' theory is appropriate, $\eta \cong h$, so that

$$R_\varepsilon(x,x';h) \equiv -\frac{1}{\pi}\log\tanh\left(\frac{\pi}{4h}\left|\int_x^{x'}\frac{dr}{1+\varepsilon}\right|\right) . \tag{2.34}$$

For shallow water we have $\varepsilon = O(kh\cdot ka)$ and we can put $\varepsilon = 0$ (Boussinesq approximation). Then:

[2] With $F_k = \left(\eta^{-1}D^k\eta\right)/\eta = \left[(\eta\partial_x)^k\right]\eta$ we have $F_1 = (1/\eta)\eta\partial_x\eta = \eta_x$ and $F_2 = \left[(1/\eta)(\eta\partial_x)^2\right]\eta = \partial_x(\eta\partial_x)\eta$ and thus, $F_2 = \eta_x^2 + \eta\eta_{xx}$. For F_3 we have $F_3 = \partial_x(\eta\partial_x(\eta\partial_x))\eta$, yielding $F_3 = \left[\eta_x^2\partial_x + 3\eta\eta_x\partial_x^2 + \eta\eta_{xx}\partial_x + \eta^2\partial_x^2\right]\eta$.

$$R_0(x,x';\eta) \equiv -\frac{1}{\pi}\log\tanh\left(\frac{\pi}{4h}\left|\int_x^{x'}\frac{dr}{1+\frac{\zeta}{h}}\right|\right) . \tag{2.35}$$

The advantage of a Hamiltonian model based on (2.35) over a Boussinesq-type model is that in the former model the linear theory is recovered in case of deep water. For practical applications, such as the evolution of a solitary wave over an uneven bottom, numerical solution of the resulting integral equations is needed (see Zwartkruis, 1991).

2.3 The evolution equations

In the following we describe the evolution equations in the physical plane including the short-wave nonlinearity function ε which depends on η and its derivatives. Thereafter, we look at the possibility of the evolution equations in the transformed plane.

2.3.1 Equations in the physical plane

Surface elevation ζ

To obtain the evolution equations it is necessary to evaluate the variational derivatives. Using the general formulation

$$\frac{\delta\mathcal{H}}{\delta\varphi} \equiv \frac{\partial H}{\partial\varphi} - \frac{\partial}{\partial x}\left(\frac{\partial H}{\partial\varphi_x}\right) - \cdots \tag{2.36}$$

we note for the Hamiltonian $\mathcal{H}$, given by (2.17), that

$$\begin{aligned}\frac{\partial\zeta}{\partial t} = \frac{\delta\mathcal{H}}{\delta\varphi} &\equiv -\frac{\partial}{\partial x}\left(\frac{\partial H}{\partial\varphi_x}\right) - \frac{\partial}{\partial x'}\left(\frac{\partial H}{\partial\varphi_{x'}}\right)\\ &= -\frac{\partial}{\partial x}\int dx'\frac{\varphi_{x'}}{2}R_\varepsilon(x,x';\eta(x)) - \frac{\partial}{\partial x'}\int dx\frac{\varphi_x}{2}R_\varepsilon(x,x';\eta(x))\\ &= -\int dx'\varphi_{x'}\frac{\partial R_\varepsilon}{\partial x} - \int dx\varphi_x\frac{\partial R_\varepsilon}{\partial x'} .\end{aligned} \tag{2.37}$$

Due to the symmetry of $R_\varepsilon(x,x';\eta)$ with respect to x and x', (2.37) can also be expressed as

$$\frac{\partial\zeta}{\partial t} = -\frac{\partial}{\partial x}\int dx'\varphi_{x'}R_\varepsilon(x,x';\eta(x)) = -\int dx'\varphi_{x'}\frac{\partial R_\varepsilon}{\partial x} . \tag{2.38}$$

The differentiation of R_ε proceeds as follows. We introduce the notation

$$v = |\vartheta| = \left|\int_x^{x'}\frac{dr}{(1+\varepsilon)\,\eta(r)}\right| .$$

From R_ε given in (2.16) we have $\mathcal{R}_\varepsilon = -\frac{1}{\pi}\log\tanh\frac{\pi}{4}v$ and thus,

$$\frac{\partial R_\varepsilon}{\partial x} = -\frac{1}{2}\frac{dv/dx}{\sinh\left(\frac{\pi}{2}v\right)} .$$

With $\frac{dv}{dx} = \mathrm{sign}(\vartheta)\frac{d\vartheta}{dx}$ and $\frac{d\vartheta}{dx} = -\frac{1}{(1+\varepsilon)\,\eta(x)}$ we obtain

$$\frac{\partial R_\varepsilon}{\partial x} = \frac{1}{2\,(1+\varepsilon)\,\eta(x)}\,\frac{\mathrm{sign}(\vartheta)}{\sinh\left(\frac{\pi}{2}v\right)} . \tag{2.39}$$

Consider now the term $\mathrm{sign}(\vartheta)/\sinh\left(\frac{\pi}{2}v\right)$:

$$\begin{aligned}\frac{\mathrm{sign}\,(\vartheta)}{\sinh\left(\frac{\pi}{2}v\right)} = \frac{\mathrm{sign}\,(\vartheta)}{\sinh\left(\frac{\pi}{2}\,|\vartheta|\right)} &= \frac{+1}{\sinh\left(\frac{\pi}{2}\vartheta\right)} && \text{if} \quad \vartheta > 0\\ &= \frac{-1}{\sinh\left(-\frac{\pi}{2}\vartheta\right)} = \frac{1}{\sinh\left(\frac{\pi}{2}\vartheta\right)} && \text{if} \quad \vartheta < 0 .\end{aligned}$$

We can therefore write

$$\begin{aligned}\frac{\partial R_\varepsilon}{\partial x} &= \frac{1}{2\,(1+\varepsilon)\,\eta(x)}\,\frac{1}{\sinh\left(\frac{\pi}{2}\vartheta\right)}\\ &= \frac{1}{2\,(1+\varepsilon)\,\eta(x)}\,\frac{1}{\sinh\left(\frac{\pi}{2}\int_x^{x'}\frac{dr}{(1+\varepsilon)\eta(r)}\right)}\end{aligned} \tag{2.40}$$

The evolution equation for the free surface elevation ζ finally becomes

$$\frac{\partial\zeta}{\partial t} = -\frac{1}{2\,(1+\varepsilon)\,\eta(x)}\int_{-\infty}^{\infty} dx'\,\frac{\varphi_{x'}}{\sinh\left(\frac{\pi}{2}\int_x^{x'}\frac{dr}{(1+\varepsilon)\eta(r)}\right)} . \tag{2.41}$$

Velocity potential φ

The evolution equation for the free surface wave potential φ is more difficult to obtain. This is due to the fact that $\varepsilon(x,t)$ is a function of $\eta(x,t)$ and therefore also a function of $\zeta(x,t)$. Since h is only a variable constant,

$$\delta\eta = \delta h + \delta\zeta = \delta\zeta . \tag{2.42}$$

Thus, $\delta\zeta$ may be replaced by $\delta\eta$. Next, $\delta\mathcal{H}$, the increment in the Hamiltonian due to $\delta\eta$, a small increment in η and the associated $\delta\varepsilon$ can be expressed as

$$\delta\mathcal{H} = \int_{-\infty}^{\infty}\left(\frac{\delta\mathcal{H}}{\delta\zeta}\delta\zeta\right)dx'$$

$$= \int_{-\infty}^{\infty} g\zeta\delta\zeta dx' - \frac{1}{4}\int_{-\infty}^{\infty} dx' \int_{-\infty}^{\infty} dx'' \frac{\varphi_{x'}\varphi_{x''}}{\sinh\frac{\pi}{2}\left|\int_{x'}^{x''}\frac{dr}{(1+\varepsilon)\eta}\right|}\delta\eta\frac{\delta}{\delta\eta}\left|\int_{x'}^{x''} dr\frac{1}{(1+\varepsilon)\eta}\right|. \quad (2.43)$$

Since $\frac{|\theta|}{\sinh\frac{\pi}{2}|\theta|} = \frac{\theta}{\sinh\frac{\pi}{2}\theta}$ one has from (2.43)

$$\begin{aligned}\delta\mathcal{H} &= \int_{-\infty}^{\infty} g\zeta\delta\zeta dx' - \frac{1}{4}\int_{-\infty}^{\infty} dx' \int_{-\infty}^{\infty} dx'' \frac{\varphi_{x'}\varphi_{x''}}{\sinh\frac{\pi}{2}\left(\int_{x'}^{x''}\frac{dr}{(1+\varepsilon)\eta}\right)}\delta\eta\frac{\delta}{\delta\eta}\left(\int_{x'}^{x''} dr\frac{1}{(1+\varepsilon)\eta}\right)\\ &= \int_{-\infty}^{\infty} g\zeta\delta\zeta dx' + \frac{1}{4}\int_{-\infty}^{\infty} dx' \int_{-\infty}^{\infty} dx'' \frac{\varphi_{x'}\varphi_{x''}}{\sinh\frac{\pi}{2}\left(\int_{x'}^{x''}\frac{dr}{(1+\varepsilon)\eta}\right)}\int_{x'}^{x''} dr\frac{(1+\varepsilon)\delta\eta+\eta\delta\varepsilon}{(1+\varepsilon)^2\eta^2}. \quad (2.44)\end{aligned}$$

One may proceed from here to derive a suitable expression by carrying out integration by parts of the right-hand side. Alternatively, a similar approach as used in appendix E of Radder (1992) may be adopted. Since (2.44) must hold for all $\delta\eta \in C$, $\delta\eta$ may be replaced by any sequence $f_n(x)$ approaching the delta function $\delta(x)$.

The following properties related to the delta function will be useful during the derivation. First, as in Radder (1992, Appendix E), use will be made of

$$\int_{x'}^{x''} drF(r)\delta(r-x) = F(x)U(x-x')U(x''-x) \quad (2.45)$$

where $F(x)$ represents a well-behaved function and $U(x)$ the unit Heaviside function. We further use the fact that (*e.g.*, Greenberg, 1978; p. 71)

$$\int_{x'}^{x''} drF(r)\delta_j(r-x) = (-1)^j F_j(x)U(x-x')U(x''-x). \quad (2.46)$$

The subscript j in (2.46) denotes the order of differentiation of the function. We now turn to evaluate $\delta\varepsilon$. Using (2.32) for ε and carrying out the operation to $O(ka)^2$, we have

$$\delta\varepsilon(r) = -\frac{1}{3}(2\eta_r\delta\eta_r + \eta\delta\eta_{rr} + \eta_{rr}\delta\eta) - \cdots . \quad (2.47)$$

Approximating $\delta\eta(r)$ by $\delta(r-x)$ in (2.47), one has

$$\delta\varepsilon = -\frac{1}{3}\left[2\eta_r\delta_1(r-x) + \eta\delta_2(r-x) + \eta_{rr}\delta(r-x)\right] - \cdots . \quad (2.48)$$

Hence,

$$\int_{x'}^{x''} dr \frac{(1+\varepsilon)\delta\eta + \eta\delta\varepsilon}{(1+\varepsilon)^2\eta^2} = \int_{x'}^{x''} dr \left[\frac{\delta\eta}{(1+\varepsilon)\eta^2} + \frac{\delta\varepsilon}{(1+\varepsilon)^2\eta}\right] = U(x-x')U(x''-x)B_1(x) \tag{2.49}$$

where B_1 up to O $[(ka)^2]$ is given by

$$B_1(\eta,\varepsilon) = \frac{1}{(1+\varepsilon)\eta^2} + -\frac{1}{3}\left[\frac{\eta\eta_{xx}}{(1+\varepsilon)^2\eta^2} - \frac{\partial}{\partial x}\left(\frac{2\eta\eta_x}{(1+\varepsilon)^2\eta^2}\right) + \frac{\partial^2}{\partial x^2}\left(\frac{\eta^2}{(1+\varepsilon)^2\eta^2}\right)\right] \tag{2.50}$$

by using a reduced form of $\varepsilon(x)$; *i.e.*,

$$\varepsilon(x,t) = -\frac{1}{3}\left(\eta_x^2 + \eta\eta_{xx}\right) . \tag{2.51}$$

Using (2.49) in (2.44) yields

$$\frac{\delta\mathcal{H}}{\delta\zeta} = g\zeta + \frac{B_1}{4}\int_{-\infty}^{\infty} dx' \int_{-\infty}^{\infty} dx'' \frac{\varphi_{x'}\varphi_{x''}}{\sinh\frac{\pi}{2}\left|\int_{x'}^{x''}\frac{dr}{(1+\varepsilon)\eta}\right|} U(x-x')U(x''-x) . \tag{2.52}$$

Rewriting the integral on the second line of (2.52), we obtain

$$\frac{\delta\mathcal{H}}{\delta\zeta} = g\zeta + \frac{B_1}{2}\int_{-\infty}^{x} dx' \int_{x}^{\infty} dx'' \frac{\varphi_{x'}\varphi_{x''}}{\sinh\frac{\pi}{2}\left(\int_{x'}^{x''}\frac{dr}{(1+\varepsilon)\eta}\right)} . \tag{2.53}$$

Consequently, the resulting evolution equation for φ is

$$\frac{\partial\varphi}{\partial t} = -\frac{\delta\mathcal{H}}{\delta\zeta} = = -g\zeta - \frac{1}{2}B_1(\eta,\varepsilon)\int_{-\infty}^{x} dx' \int_{x}^{\infty} dx'' \frac{\varphi_{x'}\varphi_{x''}}{\sinh\left(\frac{\pi}{2}\int_{x'}^{x''}\frac{dr}{(1+\varepsilon)\eta(r)}\right)} . \tag{2.54}$$

It may be noted that equation (72b) of Radder (1992) results as a special case of (2.54) for $\varepsilon = 0$.

2.3.2 Exact evolution equations

As discussed so far approximations have to be used for the inverse transformation in order to express the evolution equations in the physical plane. An alternative is to investigate the workability of using the exact equation on the transformed plane. The

exact Hamiltonian $\mathcal{H}$ and $\mathcal{R}(\chi,\chi')$ are given respectively by (2.9) and (2.10).

Surface elevation ζ

For the evaluation of $\delta\mathcal{H}/\delta\varphi$ we need only the kinetic energy part and we have

$$\frac{\delta\mathcal{H}}{\delta\varphi} = \frac{\delta\mathcal{T}}{\delta\varphi} .$$

Since the variable χ depends on η, we need to rewrite the exact expression of $\mathcal{T}$ partly in terms of the physical variable x to be able to obtain the variational derivative $\delta\mathcal{T}/\delta\varphi$. Observing that $d\chi'\varphi_{\chi'} = dx'\varphi_{x'}$, we have

$$\mathcal{T} = \frac{1}{2}\int dx\varphi_x \int dx'\varphi_{x'} R(\chi',\chi;\eta) . \tag{2.55}$$

Since $\mathcal{T}$ has no explicit dependence φ itself, we have $\dfrac{\delta\mathcal{T}}{\delta\varphi} = -\dfrac{\partial}{\partial x'}\left(\dfrac{\partial\mathcal{T}}{\partial\varphi_{x'}}\right) - \dfrac{\partial}{\partial x}\left(\dfrac{\partial\mathcal{T}}{\partial\varphi_x}\right)$ and we obtain

$$\frac{\delta\mathcal{T}}{\delta\varphi} = -\frac{\partial}{\partial x}\int_{-\infty}^{\infty} dx'\varphi_{x'}\mathcal{R}(\chi,\chi') . \tag{2.56}$$

Along the free surface $\xi = 1$ we have $\dfrac{\partial}{\partial x} = \dfrac{d\chi}{dx}\dfrac{\partial}{\partial\chi}$ and therefore $\delta\mathcal{H}/\delta\varphi$ can be exactly expressed as

$$\frac{\partial\zeta}{\partial t} = \frac{\delta\mathcal{H}}{\delta\varphi} = -\frac{d\chi}{dx}\frac{\partial}{\partial\chi}\int_{-\infty}^{\infty} d\chi'\varphi_{\chi'}\mathcal{R}(\chi,\chi') . \tag{2.57}$$

Since one has $\dfrac{d\chi}{dx} = \left(\dfrac{dx}{d\chi}\right)^{-1}$ subject to the condition that the Jacobian is not zero (which is true for the mapping used), $d\chi/dx$ can be calculated exactly from (2.12) or for a horizontal bottom from (2.18). Thus, (2.57) defines the evolution equation for ζ exactly in the transformed variables.

Velocity potential φ

The exact evolution equation for φ follows from the free surface conditions to be

$$\frac{\partial\varphi}{\partial t} = -\frac{1}{2}\varphi_x^2 + \frac{1}{2}\frac{(\zeta_t + \varphi_x\zeta_x)^2}{1+\zeta_x^2} - g\zeta \tag{2.58}$$

where again all the derivatives can be expressed in the transformed plane by using the Jacobian of the transformation.

An important point to note is that the evolution rates, given by (2.57) and (2.58), correspond to the rates at a fixed physical location x and not at a fixed χ. A fixed χ-node does not correspond to the same x-location due to the change in the surface elevation with time. For this reason, the numerical values need to be mapped from the set of χ-nodes to the set of the fixed x-locations and *vice-versa* at each time-step. This is one of the basic disadvantages of using the exact evolution equations on the χ-space.

3 Numerical evaluation of the time-domain model

In the present chapter, we describe the numerical model which is based on the formulations in the physical plane. The numerical model described here will be later referred to as '**hamilT**'.

3.1 Regularised evolution equations

As the integrands in (2.38) and (2.54) are singular at $x = x'$, regularised forms are first derived in a way similar to the one adopted in Zwartkruis (1991). Further, we derive a modified form of (2.54) where the outer double integrals need not be numerically evaluated.

Surface elevation ζ

With

$$\begin{aligned} v(x) &= \frac{\partial \varphi}{\partial x} \\ \lambda(x', x) &= v(x') - \frac{[(1+\varepsilon)\,\eta]\,(x)}{[(1+\varepsilon)\,\eta]\,(x')} v(x) \\ f(\eta, \varepsilon) &= \frac{\pi}{4} \int_x^{x'} \frac{dr}{(1+\varepsilon)\,\eta} \end{aligned}$$

we write

$$\int_{-\infty}^{\infty} dx' \lambda(x', x) \log\tanh|f(\eta,\varepsilon)| = \int_{-\infty}^{\infty} dx' v(x') \log\tanh|f(\eta,\varepsilon)| - [v(1+\varepsilon)\eta](x) \int_{-\infty}^{\infty} dx' \frac{\log\tanh|f(\eta,\varepsilon)|}{[(1+\varepsilon)\eta](x')} . \quad (3.1)$$

It follows from the definition of $f(\eta, \varepsilon)$ by using Leibnitz's rule that

$$\frac{df}{dx'} = \frac{\pi}{4} \frac{1}{(1+\varepsilon)\eta}(x') . \quad (3.2)$$

Noting that $f \to \infty$ as $x' \to \infty$ and $f \to -\infty$ as $x' \to -\infty$ we can further write

$$\begin{aligned} \int_{-\infty}^{\infty} dx' \frac{1}{[(1+\varepsilon)\eta](x')} \log\tanh|f(x,x')| &= \frac{4}{\pi} \int_{-\infty}^{\infty} df \log\tanh|f(x,x')| \\ &= -\pi . \end{aligned} \quad (3.3)$$

Using (3.3) in (3.1) yields

$$\int_{-\infty}^{\infty} dx'\lambda(x',x)\log\tanh\left|f(x,x')\right| = \pi[v(1+\varepsilon)\eta](x) + \int_{-\infty}^{\infty} dx'v(x')\log\tanh\left|f(x,x')\right| . \quad (3.4)$$

Alternatively,

$$\int_{-\infty}^{\infty} dx'v(x')\log\tanh\left|f(x,x')\right| = -\pi[v(1+\varepsilon)\eta](x) + \int_{-\infty}^{\infty} dx'\lambda(x',x)\log\tanh\left|f(x,x')\right| . \quad (3.5)$$

The integrand $\lambda(x',x)\log\tanh|f(x,x')|$ is regular at $x=x'$ and the numerical integration of the right hand side of (3.5) can be carried out by using a standard numerical technique like trapezoidal rule (or Gauss-quadrature for higher accuracy). Thus, the starting equation for the numerical evolution of the free surface is

$$\zeta_t = \frac{1}{\pi}\frac{d}{dx}\left[-\pi[v(1+\varepsilon)\eta](x) + \int_{-\infty}^{\infty} dx'\lambda(x',x)\log\tanh\left|f(x,x')\right|\right] . \quad (3.6)$$

Velocity potential φ

The double integral and the singular behaviour of the denominator at $x'=x''$ in (2.54) make a direct numerical implementation difficult. Expression (2.54) is further simplified as follows. Differentiation of (2.54) w. r. t. to x gives

$$\varphi_{tx} = -g\zeta_x - \frac{1}{2}\left[\frac{dB_1}{dx}\right]\int_{-\infty}^{x} dx'\int_{x}^{\infty} dx''g(x',x'') - \frac{1}{2}B_1\frac{d}{dx}\int_{-\infty}^{x} dx'\int_{x}^{\infty} dx''g(x',x'') \quad (3.7)$$

where

$$g(x',x'') = \frac{\varphi_{x'}\varphi_{x''}}{\sinh\frac{\pi}{2}\left(\int_{x'}^{x''}\frac{dr}{(1+\varepsilon)\eta}\right)}. \quad (3.8)$$

Using Leibnitz's rule, one has

$$\frac{d}{dx}\int_{-\infty}^{x} dx'\int_{x}^{\infty} dx''g(x',x'') = \int_{-\infty}^{x} dx'\frac{d}{dx}\int_{x}^{\infty} dx''g(x',x'') + \int_{x}^{\infty} dx''g(x,x'') = \int_{-\infty}^{x} dx'[-g(x',x)] + \int_{x}^{\infty} dx''g(x,x'') \quad (3.9)$$

It follows from the definition of g that

$$g(x',x) = -g(x,x'). \tag{3.10}$$

Hence,

$$\begin{aligned} \frac{d}{dx}\int_{-\infty}^{x} dx' \int_{x}^{\infty} dx'' g(x',x'') &= \int_{-\infty}^{x} dx'[-g(x',x)] + \int_{x}^{\infty} dx'' g(x,x'') \\ &= \int_{-\infty}^{\infty} dx' g(x,x'). \end{aligned} \tag{3.11}$$

We recall from (2.41) that

$$\int_{-\infty}^{\infty} dx' g(x,x') = -2(1+\varepsilon)\eta\varphi_x\zeta_t. \tag{3.12}$$

Using (3.11) and (3.12) in (3.7) we get

$$\begin{aligned} \varphi_{tx} &= -g\zeta_x + \left[\frac{dB_1}{dx}\right]\int_{-\infty}^{x} dx'(1+\varepsilon)\eta\varphi_{x'}\zeta_t \\ &\quad + B_1(1+\varepsilon)\eta\varphi_x\zeta_t. \end{aligned} \tag{3.13}$$

Substituting v for φ_x, (3.13) is finally expressed as

$$v_t = -g\zeta_x + \left[\frac{dB_1}{dx}\right]\int_{-\infty}^{x} dx' \left[v(1+\varepsilon)\eta\zeta_t\right] + B_1\left[v(1+\varepsilon)\eta\zeta_t\right]. \tag{3.14}$$

Expression (3.14) is the starting equation for the numerical evolution of v (or consequently of φ). The regularised set of equations is then given by

$$\zeta_t = \frac{1}{\pi}\frac{d}{dx}\left[-\pi[v(1+\varepsilon)\eta](x) + \int_{-\infty}^{\infty} dx'\lambda(x',x)\log\tanh\left|f(x,x')\right|\right] \tag{3.15a}$$

$$v_t = -g\zeta_x + \left[\frac{dB_1}{dx}\right]\int_{-\infty}^{x} dx' \left[v(1+\varepsilon)\eta\zeta_t\right] + B_1\left[v(1+\varepsilon)\eta\zeta_t\right]. \tag{3.15b}$$

In the numerical code '**hamilT**', the derivatives in the evolution equations are determined by using a fourth-order mid-point rule[1] and the integration is carried out according to the trapezoidal rule. Nodes are uniformly distributed over the entire domain.

3.2 Time integration

Time integration of the two evolution equations (3.15a) and (3.15b) are performed according to either an explicit scheme (Euler) or a predictor-corrector scheme (Adams-

[1] A Lagrangian polynomial approximation based on discrete values at 5 nodes are used, with the node of interest being the middle one. Higher-order interpolation can also be later implemented.

Bashford-Moulton, henceforth referred to as 'ABM'). From known values of ζ and v at an instant t, values at the next instant Δt later are given in the Euler procedure by

$$\zeta(x,t+\Delta t) = \zeta(x,t) + \Delta t \frac{\partial \zeta(x,t)}{\partial t} + O(\Delta t)^2 \tag{3.16}$$

$$v(x,t+\Delta t) = v(x,t) + \Delta t \frac{\partial v(x,t)}{\partial t} + O(\Delta t)^2 \tag{3.17}$$

where ζ_t and v_t are computed from the evolution equations (3.15a) and (3.15b).

For an ordinary differential equation $dy/dt = f(y,t)$, the value of y Δt later is given by a two-step procedure in the ABM scheme:

$$y^{1p} = y^0 + \frac{\Delta t}{24}\left(55y_t^0 - 59y_t^{-1} + 37y_t^{-2} - 9y_t^{-3}\right) \tag{3.18a}$$

$$y^1 = y^0 + \frac{\Delta t}{24}\left(9y_t^{1p} + 19y_t^0 - 5y_t^{-1} + y_t^{-2}\right) \tag{3.18b}$$

where the superscripts denote the number of time-steps with respect to the present instant, $1p$ being the predicted value and 1 the corrected one. In the context of the present evolution equations, the predicted values of ζ and v are evaluated first. The evolution rates ζ_t^{1p} and v_t^{1p} are then calculated from (3.15a) on the basis of the calculated ζ^{1p} and v^{1p}. Since evolution rates from three previous time-steps are used in the ABM procedure, the explicit Euler scheme is used for a few time-steps at the start of the computation. For this purpose, a much smaller time-step (four times smaller) is used than the intended time-step to be eventually used with the ABM scheme. We note that the truncation error is of $O\left(\Delta t^2\right)$ in the Euler scheme while that of the ABM scheme is $O\left(\Delta t^5\right)$.

3.3 The choice of step size

The guidelines to choose step sizes are as follows. The spatial step Δx is chosen first based on some important physical length scale of the problem. The time step Δt then follows by considering a Courant-Friedrichs-Lewy (CFL) condition: $c\Delta t < \Delta x$, or, for restricted depth,

$$\mathrm{CFL} = \sqrt{gh}\frac{\Delta t}{\Delta x} < 1\ . \tag{3.19}$$

The value of Δt depends on the integration method. We now take
Euler CFL ≤ 0.5
ABM CFL ≤ 0.8 .
We use ABM integration more or less standardly.

For problems of solitary waves, the grid size may be determined on the basis of the water depth h. An indicative value of $\Delta x/h$ for moderately high solitary waves is $1/5$.

The step-size may also be based on the *width* of the solitary wave. With

$$\zeta(x,t) = H \operatorname{sech}^2\left(\frac{x-ct}{\Delta}\right) \tag{3.20}$$

the width Δ can be estimated from[2].

$$\Delta = \sqrt{\frac{4h^3}{3H}}\,. \tag{3.21}$$

As an example, for the case of a solitary wave with height $H = 4$ m progressing on water of depth $h = 10$ m, we have $\Delta = 18.3$ m. Choosing $\Delta x = 2$ m, we then have 9 mesh points over the width of the solitary wave. Correspondingly, $\Delta t \leq 0.16$ s.

For periodic waves the smallest wave length of interest should be considered. Consider, for example, a submerged bar with the water depth changing from 0.40 m at the toe to 0.10 m at the top and an incident train of period 2.02 s. Usually the third-harmonic component, which is generated through nonlinearity, is of importance for such problems. We have the following wave lengths λ_i for the four harmonics with period $T_i = T/i$ at 0.10 m and 0.40 m depth.

h \ T_i	2.02	1.01	0.67	0.505
0.40	3.74	1.49	0.70	0.39
0.10	1.97	0.93	0.56	0.37

Table 3.1: Wave lengths λ_i for the harmonics $T_i = T/i$, $i = 1, \ldots, 4$.

With $\Delta x = 0.10$ m we have 5 points per wave length for the third harmonic at the shallower part. A sensitivity test shows the difference between choices of $\Delta x = 0.1$ m and $\Delta x = 0.05$ m. For the smaller Δx the representation of the smaller features seems to be more accurate than for the larger Δx. The general picture of the two wave profiles is the same in both cases.

[2]For solitary waves as resulting from different one-way equations, the precise form of the width Δ and the celerity c may differ, but these differences are not large (Dingemans, 1994b, section 6.3)

4 Spectral approach

In the present chapter, we discuss spectral or pseudo-spectral solution of the nonlinear water wave propagation based on the explicit Hamiltonian model. One of the basic ideas behind a spectral solution is to improve the numerical efficiency of the solution by achieving higher spatial resolution with a few spectral parameters. We had seen that using a Fourier series over a finite span was not feasible in connection with the present Hamiltonian formulations. On the other hand, the constraint of finite energy and the restriction of the initially specified disturbance to finite span points to the sinc-series as a natural choice. We discuss several possibilities of the numerical method using the sinc approximation.

4.1 Method A: x-space

We recall from section 3.1 that the (regularised) evolution equations including the short-wave nonlinearity ε are:

$$\zeta_t = \frac{1}{\pi}\frac{d}{dx}\left[-\pi\left[v(1+\varepsilon)\eta\right](x) + \int_{-\infty}^{\infty} dx'\lambda(x',x)\log\tanh\left|f(x,x')\right|\right]. \quad (4.1a)$$

$$v_t = -g\zeta_x + \left[\frac{d}{dx}B_1\right]\int_{-\infty}^{x} dx'\left[v(1+\varepsilon)\eta\zeta_t\right] + B_1\left[v(1+\varepsilon)\eta\zeta_t\right]. \quad (4.1b)$$

In the simplest adoption of sinc-series, $\zeta(x)$ and $v(x)$ in (4.1a) and (4.1b) can be approximated through the cardinal series:

$$\zeta(x,t) = \sum_{j=0}^{n}\zeta_j(t)\,\mathrm{sinc}\left(\frac{x-x_j}{\Delta x}\right), \quad (4.2a)$$

$$v(x,t) = \sum_{j=0}^{n}v_j(t)\,\mathrm{sinc}\left(\frac{x-x_j}{\Delta x}\right). \quad (4.2b)$$

Further simplification is achieved by recognising that the function $\lambda(x',x)\log\tanh|f(x,x')|$ belongs to the Paley-Wiener class of $B(\Delta x)$ (Lund and Bowers, 1992; chapter 2) and hence can be expressed by the sinc-series, *i.e.*

$$\lambda(x',x)\log\tanh\left|f(x,x')\right| = \sum_{j=0}^{n}\lambda_j^*(x)\,\mathrm{sinc}\left(\frac{x'-x_j}{\Delta x}\right) \quad (4.3)$$

where

$$\begin{aligned}\lambda_j^*(x) &= 0, \quad [x = j\Delta x] \\ &= \left(v(j) - \frac{[(1+\varepsilon)\eta](x)}{(1+\varepsilon_j)\eta_j} v(x)\right) \log\tanh|f(x,x_j)| \quad [x \neq j\Delta x]\,. \end{aligned} \tag{4.4}$$

Introducing the expression (4.3) into (4.1a) and using the integral relation (*e.g.*, Lund and Bowers, 1992; p25)

$$\int_{-\infty}^{\infty} \operatorname{sinc}\left(\frac{x'-x_j}{\Delta x}\right) dx' = \Delta x \tag{4.5}$$

yields the following simplified evolution equation for surface elevation:

$$\zeta_t = \frac{1}{\pi}\frac{d}{dx}\left[-\pi[v(1+\varepsilon)\eta](x) + \Delta x \sum_{j=0}^{n} \lambda_j^*\right]. \tag{4.6}$$

The replacement of (4.1a) through (4.6) is in fact the same as the trapezoidal integration. However, the formalism of the sinc series under the assumption that the function $\lambda(x', x)\log\tanh|f(x, x')|$ belongs to the Paley-Wiener class of $B(\Delta x)$ gives justification to the exactness of (4.6).

In the integral over $(-\infty,\ x]$ in (4.1b) we note that the combined function $v(1+\varepsilon)\eta\zeta_t$ can be approximated through the orthogonal sinc series since $v, \zeta_t \in B(\Delta x)$ while $(1+\varepsilon)$ and η are bounded (O(1)). Introducing the series

$$v(1+\varepsilon)\eta\zeta_t(x') = \sum_{j=0}^{n} [v(1+\varepsilon)\eta\zeta_t]_j \operatorname{sinc}\left(\frac{x'-x_j}{\Delta x}\right) \tag{4.7}$$

into (4.1b) results in the following simplified evolution equation for v:

$$\begin{aligned} v_t &= -g\zeta_x + B_1[v(1+\varepsilon)\eta\zeta_t] \\ &\quad + \left[\frac{d}{dx}B_1\right] \sum_{j=0}^{n} [v(1+\varepsilon)\eta\zeta_t]_j \int_{-\infty}^{x} dx' \operatorname{sinc}\left(\frac{x'-x_j}{\Delta x}\right). \end{aligned} \tag{4.8}$$

Note that for $x = k\Delta x$ and $x_j = j\Delta x$ the integral

$$\begin{aligned} \int_{-\infty}^{x} dx' \operatorname{sinc}\left(\frac{x'-x_j}{\Delta x}\right) &= \int_{-\infty}^{x_j} dx' \operatorname{sinc}\left(\frac{x'-x_j}{\Delta x}\right) + \int_{x_j}^{x} dx' \operatorname{sinc}\left(\frac{x'-x_j}{\Delta x}\right) \\ &= \frac{\Delta x}{2} + \frac{\Delta x}{\pi}\int_0^{\pi(k-j)} \frac{\sin\theta}{\theta} d\theta \end{aligned} \tag{4.9}$$

is time invariant and can be easily computed.

4.2 Method A: χ-space

One of the disadvantages of the method using (4.6) is associated with the evaluation of the integral function $f(x, x_j)$ appearing in λ_j^*. This can be avoided by using the evolution equations in χ-space (Radder, 1992) given by:

$$\dot{m} = \frac{1}{\pi}\int_{-\infty}^{\infty} d\chi' v(\chi') \log\tanh\frac{\pi}{4}|\chi-\chi'| \tag{4.10a}$$

$$\dot{\varphi} = -g\zeta - \frac{B_1}{2}\int_{-\infty}^{\chi} d\chi' \int_{\chi}^{\infty} d\chi'' \frac{v(\chi')v(\chi'')}{\sinh\frac{\pi}{2}|\chi'-\chi''|} \tag{4.10b}$$

Under the assumption that the short-wave nonlinearity $\varepsilon = 0$, we have

$$B_1 = \frac{1}{\eta^2}, \quad \text{and} \quad \frac{dx}{d\chi} = \eta. \tag{4.11}$$

Expressing $v(\chi)$ in sinc-series in the uniform χ-grid, the evolution equations become

$$\dot{m} = \sum_{j=0}^{n} v_j^* I_j^a(\chi) \tag{4.12a}$$

$$\dot{\varphi} = -g\zeta - \frac{B_1}{2}\sum_{j=0}^{n}\sum_{k=0}^{n} v_j^* v_k^* I_{j,k}^b(\chi) \tag{4.12b}$$

where v_j^* is the value of v at $\chi_j = j\Delta\chi$ and

$$I_j^a(\chi) = \frac{1}{\pi}\int_{-\infty}^{\infty} d\chi' \,\mathrm{sinc}\left(\frac{\chi'-\chi_j}{\Delta\chi}\right) \log\tanh\frac{\pi}{4}|\chi-\chi'|, \tag{4.13a}$$

$$I_{j,k}^b(\chi) = \int_{-\infty}^{\chi} d\chi' \int_{\chi}^{\infty} d\chi'' \frac{1}{\sinh\frac{\pi}{2}|\chi'-\chi''|} \,\mathrm{sinc}\left(\frac{\chi'-\chi_j}{\Delta\chi}\right) \mathrm{sinc}\left(\frac{\chi''-\chi_k}{\Delta\chi}\right) \tag{4.13b}$$

The integrals $I_j^a(\chi)$ and $I_{j,k}^b(\chi)$ are time-independent and can be accurately evaluated. Note, however, that the evolution rates $\dot{m}$ and $\dot{\varphi}$ are the Eulerian evolution rates and do not therefore correspond to the evolution rates at a fixed χ-grid point. This means that a correspondence between the uniform χ-grid and the x-grid has to be made at each time step unless the evolution rates of m and φ are derived at fixed χ-grid points.

4.2.1 Evolution rate at fixed χ-grids

Let $x_j^t = x(\chi_j)$. The evolution rate at a fixed χ_j is then

$$\frac{d\psi}{dt}(x_j^t) = \frac{\partial\psi}{\partial t} + \frac{\partial\psi}{\partial x}\frac{dx_j^t}{dt} \tag{4.14}$$

where $\partial\psi/\partial t$ is the Eulerian evolution rate of ψ (mass m or potential φ). The convective term can be expressed entirely in the χ-space, *i.e.*;

$$\frac{\partial\psi}{\partial x} = \frac{\partial\psi}{\partial\chi}\frac{\partial\chi}{\partial x} = \frac{1}{\eta}\frac{\partial\psi}{\partial\chi} \tag{4.15a}$$

and

$$\frac{dx_j^t}{dt} = \frac{d}{dt}\int_{-\infty}^{\chi_j}\frac{dx}{d\chi}d\chi = \frac{d}{dt}\int_{-\infty}^{\chi_j}\eta d\chi = \int_{-\infty}^{\chi_j}\zeta_t d\chi\,. \tag{4.15b}$$

4.3 Method B

In this procedure, one begins with the expression for the Hamiltonian

$$\mathcal{H} = \int_{-\infty}^{\infty}\frac{1}{2}g\zeta^2 dx - \frac{1}{2\pi}\int_{-\infty}^{\infty}dx\int_{-\infty}^{\infty}dx' v(x)v(x')\log\tanh\frac{\pi}{4}\left|\int_x^{x'}\frac{dr}{(1+\varepsilon)\eta}\right|\,. \tag{4.16}$$

Using the same sinc series (4.2a)-(4.2b), the Hamiltonian $\mathcal{H}$ can be expressed as

$$\mathcal{H} = \frac{1}{2}g\sum_{j=0}^{n}\zeta_j^2\Delta x - \frac{1}{2\pi}\sum_{j=0}^{n}\sum_{k=0}^{n}v_j v_k E(j,k,\eta) \tag{4.17}$$

where

$$E(j,k,\eta) = \int_{-\infty}^{\infty}dx\int_{-\infty}^{\infty}dx'\left[\operatorname{sinc}\left(\frac{x-x_j}{\Delta x}\right)\operatorname{sinc}\left(\frac{x'-x_k}{\Delta x}\right)\cdot \log\tanh\frac{\pi}{4}\left|\int_x^{x'}\frac{dr}{(1+\varepsilon)\eta}\right|\right]\,. \tag{4.18}$$

The basic evolution equations are then obtained from

$$\dot{m}_p = -\frac{1}{\Delta x}\frac{\partial\mathcal{H}}{\partial v_p}, \quad \dot{\varphi}_p = -\frac{1}{\Delta x}\frac{\partial\mathcal{H}}{\partial\zeta_p}. \tag{4.19}$$

Hence, from (4.17) and (4.19) one has

$$\dot{m}_p = \frac{1}{\pi(\Delta x)}\sum_j v_j E(j,p,\eta)\,, \tag{4.20a}$$

$$\dot{\varphi}_p = -g\zeta_p + \frac{1}{2\pi(\Delta x)} \sum_j \sum_k v_j v_k \frac{\partial}{\partial \zeta_p} E(j,k,\eta) \,. \tag{4.20b}$$

Basic to the efficiency of this approach is a smart evaluation of the integral related to the kinetic energy using the property of the sinc and log tanh functions.

4.4 Method C

Radder (1993a, appendix A) has shown that $\mathcal{T}$, the kinetic energy part of the total Hamiltonian, can be expressed in the form:

$$\mathcal{T} = \sum_{j=0}^{n} \sum_{k=0}^{n} v_j^* v_k^* I(|j-k|; \Delta\chi) \tag{4.21}$$

where

$$I(|j-k|; \Delta\chi) = \frac{\Delta\chi}{2} \int_0^1 d\lambda \frac{\tanh(\pi\lambda/\Delta\chi)}{\pi\lambda/\Delta\chi} \cos\left[\pi(j-k)\lambda\right] \tag{4.22a}$$

and v_j^* denotes v at the j-th point along the equidistant χ grid or in other words,

$$v(\chi) = \sum v_j^* \,\mathrm{sinc}\left(\frac{\chi - \chi_j}{\Delta\chi}\right). \tag{4.22b}$$

Note that $I(|j-k|; \Delta\chi)$ is exact (evaluated exactly on the χ-space without using any approximate transformation to x-space) and needs to be evaluated on the χ-grid once at the start of the computation. The disadvantages of using (4.22a), however, become apparent if the evolution equations are looked at.

4.4.1 Evolution equation: η

Since the pseudo-spectral variables v_j^*'s are not canonical, the evolution rates cannot be expressed as simple functional derivatives of the Hamiltonian in terms of v_j^*'s; *i.e.*, the equation

$$\dot{m}_p^* = -\frac{1}{\Delta\chi} \frac{\delta\mathcal{H}}{\delta v_p^*} = -2 \sum v_j^* I(|j-p|; \Delta\chi) \tag{4.23}$$

is not valid. On the other hand, the evolution equation for mass (consequently, surface elevation) should be determined from

$$\dot{m}_p = -\frac{1}{\Delta x} \frac{\delta\mathcal{H}}{\delta v_p} = -\frac{1}{\Delta x} \sum_j \frac{\delta\mathcal{H}}{\delta v_j^*} \frac{\delta v_j^*}{\delta v_p}. \tag{4.24}$$

The term $\left(\delta v_j^* / \delta v_p\right)$ can be evaluated from the expression

$$v_j^* = v(x_j^t) = \sum_k v_k \,\mathrm{sinc}\left(\frac{x_j^t - x_k}{\Delta x}\right) \tag{4.25}$$

where x_j^t denotes the x-coordinate of the j-th grid point on the χ-space.

4.4.2 Evolution equation: φ

The expression

$$\mathcal{V} = \frac{1}{2} g \sum \zeta_j^2 \Delta x \tag{4.26}$$

is exact for the potential energy $\mathcal{V}$ where ζ_j denotes the surface elevation from the still water level at the j-th point along the uniform $x-$grid. Using (4.26) and (4.21) the evolution equation for φ_p becomes

$$\dot{\varphi}_p = -g\zeta_p + \frac{1}{\Delta x} \sum\sum I(|j-k|;\Delta\chi) \frac{\partial}{\partial \zeta_p} v_j^* v_k^* \,. \tag{4.27}$$

We have treated the integral $I(|j-k|;\Delta\chi)$ in (4.27) invariant (on uniform χ-grid) leaving the discrete v_j^*'s to respond to increments in surface elevation ζ_j (on uniform $x-$grid). The derivative $\partial(v_j^* v_k^*)/\partial\zeta_p$ can be computed in the following way.

Let x_j^t denote the $j-th$ point on a nonuniformly distributed x-grid such that $x_j^t = x(\chi_j)$ and Δx_j^t represent the shift in x_j^t due to $\Delta\zeta_p$. $\Delta v_j^*(\zeta_p)$, the increment in v_j^* due to $\Delta\zeta_p$, is then given by

$$\Delta v_j^*(\zeta_p) = v(x_j^t + \Delta x_j^t) - v(x_j^t) = \Delta x_j^t \frac{\partial v}{\partial x}(x_j^t) + \cdots \,.$$

Thus,

$$\frac{\partial}{\partial \zeta_p} v_j^* v_k^* = \lim_{\Delta\zeta_p \to 0} \left[v_k^* \frac{\partial v}{\partial x}(x_j^t) \frac{\Delta x_j^t}{\Delta \zeta_p} + v_j^* \frac{\partial v}{\partial x}(x_k^t) \frac{\Delta x_k^t}{\Delta \zeta_p} \right] \,.$$

The order to which depth variation and surface nonlinearity are explicitly accounted for in the model depends on the form of the approximation of the actual Woods transformation. In first instance, we shall use the relation $\dfrac{dx}{d\chi} = \eta$ which gives $x(\chi) = x(\chi_0) + \displaystyle\int_{\chi}^{\chi_j} \eta d\chi$. An integral expression for $\partial x^t/\partial\zeta_p$ then results:

$$\frac{\partial x^t}{\partial \zeta_p}(j) = \int_{\chi}^{\chi_j} \frac{\partial \eta}{\partial \zeta_p} d\chi = \int_{x_0^t}^{x_j^t} \frac{\partial \eta}{\partial \zeta_p} \frac{1}{\eta} dx = \int_{x_0^t}^{x_j^t} \frac{1}{\eta} \,\mathrm{sinc}\left(\frac{x - x_p}{\Delta x}\right) dx. \tag{4.28}$$

4.5 Summary

The procedure outlined in Method A eliminates a significant amount of numerical computation by utilising the properties of sinc functions. Besides, one expects that smaller number of grid points are required than that in the previous time-domain model to achieve the same degree of accuracy. The numerical efficiency of Method B depends largely on how the integral $E(j,k,\eta)$ can be further simplified.

The procedure used in Method C has one distinct advantage from the physical point of view: the evolution equations are kept exact, the approximation being introduced only through the transformation from x to χ and *vice versa*. This allows easier modification of the numerical code to incorporate higher-order formulations. The disadvantage is related to the fact that the numerical operations are distributed over uniform x-grid and χ-grid involving continuous interpolation from one to another.

5 Numerical method using sinc-series

In the previous chapter we discussed possible formulations based on sinc method of which we set out the reasons for the choice of the evolution equations in the x-space of Method A (repeated here for convenience):

$$\zeta_t = \frac{1}{\pi}\frac{d}{dx}\left[-\pi[v(1+\varepsilon)\eta](x) + \Delta x \sum_{j=0}^{n} \lambda_j^*\right], \tag{5.1}$$

$$v_t = -g\zeta_x + B_1[v(1+\varepsilon)\eta\zeta_t] + \left[\frac{d}{dx}B_1\right]\sum_{j=0}^{n}[v(1+\varepsilon)\eta\zeta_t]_j \int_{-\infty}^{x} dx' \,\mathrm{sinc}\left(\frac{x'-x_j}{\Delta x}\right), \tag{5.2}$$

with λ^* defined in (4.4). Note that the choice of the sinc-series for the global approximation requires the grid points to be uniformly spaced and for $x_k = k\Delta x$ and $x_j = j\Delta x$, one has

$$\int_{-\infty}^{x_k} dx' \,\mathrm{sinc}\left(\frac{x'-x_j}{\Delta x}\right) = \frac{\Delta x}{2} + \frac{\Delta x}{\pi}\int_0^{\pi(k-j)} \frac{\sin\theta}{\theta} d\theta. \tag{5.3}$$

5.1 Numerical procedure

The numerical procedure proceeds in two steps: computation of the evolution rates and the time integration of the evolution. There are two available options in the code for carrying out the time integration: a first order explicit method (Euler) and a fourth order predictive-corrective method (ABM). It has been seen from previous computations using the time-domain model that much larger time steps can be successfully used while using the ABM method for the time integration of the evolution rates. The time-integration procedure is the same in both the models.

Before describing some specific aspects of the computation of the evolution rate of surface elevation, we look at two main numerical operations, involved in the computation of the evolution equations. These are integration of a function over an interval and the estimation of the derivative at a nodal point.

5.1.1 Integration procedure

Consider the evaluation of

$$I_g = \int_{x_i}^{x_{i+1}} g(x)dx \tag{5.4}$$

where x_i is the x-coordinate of the grid point i and g is an arbitrary regular function. A Gauss-quadrature procedure is implemented in order that this integral can be evaluated accurately for relatively large δx. This means that the function value needs to be known at the integration points in the interval $[x_i, x_{i+1}]$. Estimation of these values is done through a higher-order approximation based on shape-function method (see Zienkiewicz and Morgan, 1983 for the definition of shape functions). In terms of the shape functions $N_l(\mu)$'s defined in parameter μ, an approximation to the function $g(x)$ is expressed in the form

$$g(x(\mu)) = \sum_{l=1}^{l=2m} g(x_{(i-m+l)}) N_l(\mu) \tag{5.5}$$

One can now rewrite the integral I_g as

$$I_g = \sum_{l=1}^{l=2m} g_{(i-m+l)} \int_{\mu(x_i)}^{\mu(x_{i+1})} N_l(\mu) \frac{dx}{d\mu} d\mu. \tag{5.6}$$

Note that the order of the approximation is $(2m-1)$ and the approximation of the function over $x_i \leq x \leq x_{i+1}$ is based on the discrete values of the function at nodes surrounding the interval(*i.e.*, m number of nodes on either side of the interval are used for the approximation). In a general way for both uniform and nonuniform grids mapping of x to μ can take place in a similar way (known as 'isoparametric' approach) in the form

$$x(\mu) = \sum_{l=1}^{l=2m} x_{(i-m+l)} N_l(\mu) \, . \tag{5.7}$$

A simpler transformation valid only for uniformly spaced grids is

$$x(\mu) = x_{(i-m+1)} + \frac{(2m-1)\Delta x}{2}(\mu + 1) \, . \tag{5.8}$$

It is convenient to express the integral (5.6) over the interval [-1,1] for the Gauss-quadrature integrations. This is done by another transformation, defined by

$$\mu = \mu(x_i) + \frac{\mu(x_{i+1}) - \mu(x_i)}{2}(\xi + 1) \, , \tag{5.9}$$

where

$$\mu(x_i) = -\frac{1}{2m-1}, \quad \mu(x_{(i+1)}) = \frac{1}{2m-1}. \tag{5.10}$$

Finally, one has

$$I_g = \sum_{l=1}^{l=2m} g_{(i-m+l)} \int_{-1}^{1} N_l \frac{dx}{d\mu} \frac{d\mu}{d\xi} d\xi = \sum_{l=1}^{l=2m} g_{i-m+l} I_l \tag{5.11}$$

where

$$I_l = \int_{-1}^{1} N_l \frac{dx}{d\mu}\frac{d\mu}{d\xi} d\xi. \tag{5.12}$$

I_l, which is computed through Gauss-quadrature, is computed only once at the start of the computation.

5.1.2 Computation of the derivative

The derivative of a function at a grid point i is computed by interpolation from its values at the adjacent grid points from the relation:

$$f_x(i) = \sum_{l=-m}^{l=m} w_l f(i+l) \tag{5.13}$$

where the coefficients w_l's are independent of i (though dependent on Δx) for uniform grids. The order of interpolation is $2m$ (based on $2m+1$ nodes).

5.1.3 Evolution rates

Computation of the evolution rate of v from (5.2) is rather straight-forward using the integration and derivative procedures just described. Computation of the evolution rate of surface elevation needs some specific considerations.

Computation of the term λ_j^* (see Eq. (4.4)) involves the expression

$$\log\tanh|f(x_k, x_j)| = \log\tanh\left|\int_{x_j}^{x_k} \frac{dx}{(1+\varepsilon)\eta}\right| . \tag{5.14}$$

The integral argument of log tanh is evaluated through

$$\int_{x_j}^{x_k} \frac{dx}{(1+\varepsilon)\eta} = |F_k - F_j| \tag{5.15}$$

where

$$F_l = \int_{x_0}^{x_l} \frac{dx}{(1+\varepsilon)\eta}; \quad l = 1, 2, \cdots, n \tag{5.16}$$

It is further true that the value of λ_j^* decreases rapidly away from the point i due to the log tanh operator. It is possible therefore to limit the sum to smaller number of nodes, *e.g.*,

$$\sum_{j=0}^{j=n} \lambda_j^* \approx \sum_{j=i-p}^{j=i+p} \lambda_j^* \tag{5.17}$$

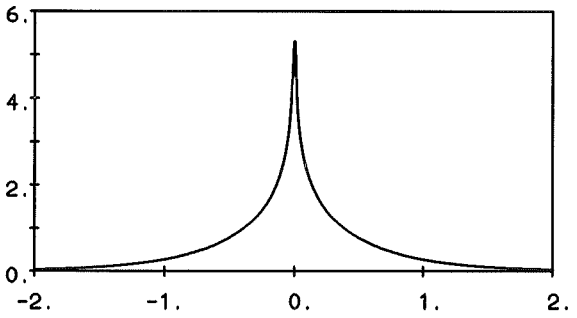

Figure 5.1: The function $\log\tanh(x)$

where the minimum value of $(i-p)$ and the maximum value of $(i+p)$ are limited by the computational grid points used. The index p at a grid-point i is calculated by using a simple criterion based on the local water depth η_i:

$$\frac{p\Delta x}{\eta_i} \geq R_l \tag{5.18}$$

where R_l is an user specified limit. The value of R_l should never be lower than 3. It is, however, safer to use a somewhat larger value (say around 10). The behaviour of the function $\log\tanh(x)$ is shown in Fig. 5.1, where it has to be understood that at $x = 0$ an asymptote is present. Here the graph is such that we stay clear from $x = 0$ by 0.005 units.

5.1.4 End treatment

The basic formulations which constitute the numerical model here are based on an infinite span. The validity of a finite computational length rests on the fact that the entire wave action is contained well within the finite span. This is difficult to meet in practice if the computations are to be run for a long time of wave propagation. A proper physical treatment of this problem, though rather important, is not yet undertaken. In the following, numerical aspects of the 'end treatment' are briefly described.

The procedures used for computing the integrals and derivatives as described earlier assume that the required number of grid points are available on either side (of an interval or a grid-point) and are therefore not strictly valid at the ends. This means that the procedures need to be modified at the ends. An attractive alternative is to define the necessary number of artificial grid-points to be able to use the same procedures for all the real nodes. Presently, the function value f at an artificial grid-point x^a is defined through the simple relation:

$$f(x^a) = f(x^e) \tag{5.19}$$

where x^e is the closest real grid-point. The artificial grid-points are also assumed to be equidistant in the same manner as the real grid points. Though the simple form (5.19) can be modified, it is not considereded really important with the assumption that the wave action should be non-significant near the ends.

5.2 The choice of step size

The choice of the spatial step size has already been discussed on physical grounds in section 3.3. In the numerical code '**sinctm**', the step-size depends on the adequacy of the global approximation through the sinc-series and further on the order of interpolation used for the evaluation of the derivatives and the local integrals. This feature can be illustrated by referring to the Figure 5.2. The top left figure shows a clear difference

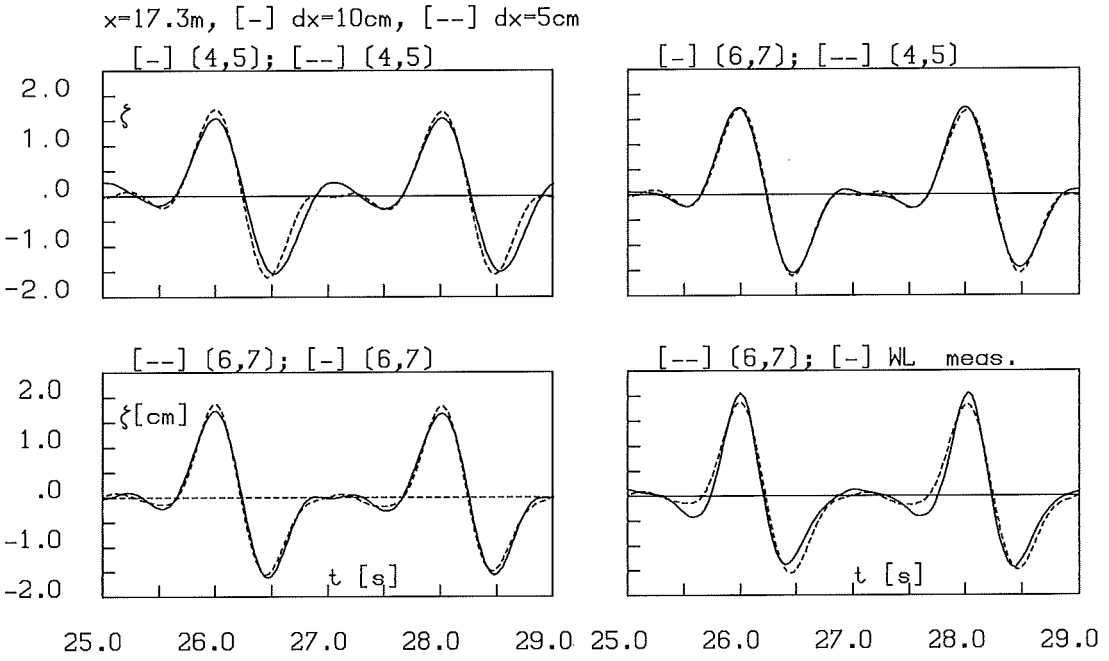

Figure 5.2: Comparison of computed and measured surface elevation at $x = 17.3$m on the back-slope of a bar (Fig. 7.27). The parameters n and m in (n, m) in the figure above denote the number of grid points used locally for the purpose of computing integration and derivative respectively. The dotted line represents the computed results with $\Delta x = 5$cm. The solid line represents the computed results with $\Delta x = 10$cm except in the bottom right where it shows the measured value in an experiment.

in the computed results with the two step-sizes. It is shown in the top right figure that this difference is made negligibly small by using a higher order local interpolation with the larger step-size. This indicates that the larger step-size is nearly sufficient for achieving an accurate global representation through the sinc-series. This is further confirmed in the bottom left figure where decreasing the step-size while still using the higher order local interpolation results in a much smaller change. It is also clear that a decrease in the step-size with the same order of interpolation or an increase in the order of interpolation with the same step-size has the desired effect of reproducing the measurement more accurately. The ratio of the time-step to the spatial step-size used during these computations is held constant. This numerical experiment strongly suggests that the required step-size could be significantly reduced by using a higher order local interpolation provided sufficiently accurate global approximation is achieved through the sinc-series.

6 The programs

6.1 The main programs

We have two main programs **hamilT** and **sinctm** and some service programs to generate input and to analyse output. With **hamilT** and **sinctm** input files with the fixed names **hamil.inp** and **sinctm.inp** are required together with files ***.ham** in which the initial wave profile and the velocity potential at the free surface are given. The ***.ham** files are generated with the program **solphi** for the generation of a solitary wave according to Tanaka's (1986) method or with **perphi** for the case of a train of period waves. Output of **hamilT** and **sinctm** consists of files ***.out** in which at selected times the ζ and φ are given as function of x, files ***.tiz** in which time series of ζ at selected stations are contained, files ***.tip** with analogous time series for φ, a file ***.ene** in which the integral measures for mass, kinetic and potential and total energy are contained for each time step. Lastly a ***.log** file is generated in which some administration is contained.

An example of a file **hamil.inp** is given below for the computation **p3**.

```
p3.ham
p3.out
p3.ene
p3.tiz
p3.tip
p3.log
p3.chk
0
2
```

Notice that the file p3.ham should exist (it is input). The file names are free, but it is recommended to use the extensions proposed so that the meaning is clear. The given sequence of file names is obligatory. The parameters 0 and 2 stand for **icleps** denoting the way nonlinearity is taken into account and the procedure for time integration respectively. For the integration method one may choose either Euler's integration (choice 1) or Adams-Bashford-Moulten (ABM) integration method (choice 2). The meaning of icleps is as follows.

We consider the following cases:
icleps=0 : $\varepsilon = 0$ and $B_1 = \dfrac{1}{\eta^2}$
icleps=1 : $\varepsilon = -\dfrac{1}{3}\left(\eta_x^2 + \eta\eta_{xx}\right)$ and B_1 according to (2.50)
icleps=2 : $\varepsilon = -\dfrac{1}{3}\left(\eta_x^2 + \eta\eta_{xx}\right)$ and $B_1 = \dfrac{1}{(1+\varepsilon)\,\eta^2}$.
Instabilities have been found to develop very soon if the parameter 'icleps' is taken to be 1.

In fact, we almost always use ABM's integration method and the option 'icleps = 0'. For a computation with name **p3** the following files are defined:

p3.ham This is the main input file for the computation. The initial value for ζ and the potential at the free surface φ are given, together with the grid x/h and the depth h. Also parameters such as Δt, Δx, the number of time steps and the number of x-steps are given. Because this file is difficult to compose, it is made by a separate program, in which the initial condition is defined together with the bottom geometry. For the different types of initial conditions we have separate programs: one for solitary waves (**solphi.for**) and one for periodic waves (**perphi.for**).

p3.out In this file the requested output is given for the wanted time steps. At time $t = 0$ and $t = nt * \Delta t$, x/h, ζ and φ are written for all mesh-points x in this file. First a line is written with "TIME STEP $= \cdots$ $Dt = \cdots$. Such output is not written for each time step but after $nwrt * \Delta t$, where $nwrt$ is given in the input. For analysis purposes, the resulting long file p3.out can be split up by using a separate program (**trans.for**), which is also delivered. The *.out file is the main output file.

p3.ene In this file the mass, kinetic, potential and total energy density is given for each time step.

p3.tiz Time signals of ζ are given at pre-selected stations.

p3.tip Time signals of φ are given at pre-selected stations (the same as those for ζ).

p3.log A file in which the computed time step is logged. Also the CPU time of the computation is given.

p3.chk A file which served as a check on some numerical tests. The use of this file is 'commented out' now, but may be needed later to test variations in the numerical scheme.

For the model **sinctm** some further input parameters are needed. An example of these is

```
4    5     8              / node appr., node derivation, integration
1   10.0                  / logtanh truncation yes, distance (x0-xh)/h
0    1   10    301        / fixed grid, number of gridpoints, number dt,
                          / last gridpoint
```

The last line is for a moving grid, which has also been made possible, but is still under investigation. The same input file .inp which is correct for **sinctm** may also be used for the program **hamilT**.

6.2 The input-generating programs solphi and perphi

In order to make the ***.ham** file, the program **solphi.for** for solitary-wave input and the program **perphi.for** for periodic wave input are available. In each of the programs the bottom-geometry is also organised. Only special forms of 1D-bottom geometries can be generated, but they are quite general. A bar can be defined in the following way. The region in x is divided in three parts: before, above, and behind the bar: w_0, w_1 and w_2. The corresponding water depths are given by h_0, h_1 and h_2. Two (mean) bottom slopes have to be given also. The depth h as function of x is given in the same way as in Dingemans et al. (1991):

$$-h(x) = h_0 + \frac{1}{2}(1+\tanh\alpha_1)\,\Delta h_1 + \frac{1}{2}(1+\tanh\alpha_2)\,\Delta h_2 \tag{6.1}$$

with

$$\alpha_j = \frac{2s_j}{\Delta h_j}(x - w_j)\ , \quad j = 1,2 \tag{6.2}$$

where Δh_1 is the change in depth over the first region of inhomogeneity and s_1 is the bottom slope in the middle (in absolute value the maximum one). The length of the computational domain is given in m by $w_1 + w_2 + w_3$ and Δx is given in the input. For the time Δt is given together with the number of time-steps, nt and the value of $nwrt$. For solphi an example of an input file is given below. In this case we have a horizontal bottom. In the example for perphi a shelf is defined.

```
#
# Inputfile voor berekeningen nov 1992
# 2 solitary waves, opposing; here the first one
#
# Time parameters : dt , Nt , Ntwrt     (1 real,2 integers)
     0.1 ,     600 ,      5
#
#Width foreland (m) , Width bar (m)    , Width hinterland (m) (format : 3 reals)
 1000.0              ,   0.0          ,  0.0
#Increment x         , Nr. of segments , (1 real,1 integer,one should be zero !)
   2.0               ,      0
#Depth foreland (m) , Deptht bar (m)   , Depth hinterland (3 positive reals)
  10.0               ,    10.0         ,   10.0
#Steepness 1st       ,  2nd slope      , (2 reals , uphill = + , downhill = - )
   0.0               ,   0.0
#Amplitude (m)       ,Maximum nr. of iterations (1 real,1 integer)
   3.                ,     50
#Plaats van top van solitaire golf in m
   700.0
 2
 350.0  650.0
```

Notice that the solitary wave so computed with solphi travels to the right (i.e., in the direction of increasing x). For the case of two opposing solitary waves of equal amplitude, the program solphi is run twice with different locations x_0 for the crest of the solitary wave. For the wave traveling in the negative $x-$direction, the value of φ in the .ham file should change. With the program **hamcom.for** the values of φ in the two files are subtracted and the ζ values are added, while the rest remains unchanged. The program hamcom.for is also delivered. For the case that the waves travel in the same $(x+)$ direction, both the ζ and the φ values in both files have to be added. (This obvious modification of hamcom is given as hamcomp.for.)

6.3 Periodic wave input

For the periodic input we use a kind of wave group composed of a number of frequencies, amplitudes and phases. The method in which a time signal of bounded variation can be defined is given in this section.

6.3.1 Introduction

Initially the evolution equations based on the Hamiltonian approach have been solved for the case that the initial value has been given by a solitary wave. The profile of this solitary wave has been computed according to Tanaka's (1986) method. We have an initial-value problem and for the computation of periodic waves in the present setting we have to comply with the initial-value problem and therefore we cannot let the wave profile coming in through the left-hand boundary so as to simulate a wave maker. We have to specify the initial wave form in x and this initial form has to be of *bounded variation.*

As a wave profile we presently have

$$\zeta(x,t) = \sum_{j=1} a_j \cos\chi_j \quad \text{with} \quad \chi_j(x,t) = k_j x - \omega_j t + \vartheta_j \ . \tag{6.3}$$

By taking the frequencies close together we have a group. As we have to have a signal of bounded variation, we should have $\zeta \to 0$ for $x \to \pm\infty$. This may be achieved by applying a taper function of the signal, i.e., we consider

$$\eta(x,0) = f(x)\zeta(x,0) \ , \tag{6.4}$$

with $f(x) = 1$ near the centre of the group and $f(x) \to 0$ for $x \to \pm\infty$ and consider the evolution of η.

For the free surface potential $\phi(x,t)$ it follows from the linear theory that

$$\Phi_j(x,z,t) = \frac{a_j g}{\omega_j} \frac{\cosh[k(z+h)]}{\cosh kh} \sin\chi_j \ . \tag{6.5}$$

We now define the free surface potential ϕ at $z = 0$, which is consistent with linear theory[1]:

$$\phi(x,t) = \Phi(x,0,t) = \frac{a_j g}{\omega_j} \sin\chi_j \ . \tag{6.6}$$

Because of the linearity, the same tapering function as used for ζ is now applied on ϕ and we get φ as

$$\varphi(x,t) = f(x)\phi(x,t) \ . \tag{6.7}$$

6.3.2 The taper function $f(x)$

As taper functions for the left and right-hand sides we take

[1] It is easily possible to define ϕ at $z = \eta$, but this is deemed not to be necessary.

$$
\begin{aligned}
f_\ell(x) &= \frac{1}{2} + \frac{1}{2}\tanh\left[b_\ell\,(x - x_\ell)\right] \\
f_r(x) &= \frac{1}{2} - \frac{1}{2}\tanh\left[b_r\,(x - x_r)\right]
\end{aligned}
\tag{6.8}
$$

Notice that as the argument of the tanh function is dimensionless and as x has the dimension of m, the coefficients b_ℓ and b_r have dimension m^{-1}. The domain $[x_\ell, x_r]$ depends on the signal used and the parameters b_ℓ and b_r control the effective width of the transition. As it is known that $\tanh \pi = .9963 \cong 1$, we should have at least $b_\ell\,(x - x_\ell) + b_r\,(x_r - x) \geq 2\pi$. With the obvious choice $b_\ell = b_r \equiv b$ this becomes

$$
b\,(x_r - x_\ell) \geq 2\pi\ . \tag{6.9}
$$

Choosing a transition width L_w with the proviso that $2L_w \leq (x_r - x_\ell)$, an initial choice for the value b follows as

$$
b \cong \pi / L_w\ . \tag{6.10}
$$

The length of a wave group

The sum of two waves is given as

$$
\zeta = \zeta_1 + \zeta_2 = a_1 \cos\chi_1 + a_2 \cos\chi_2 = a\cos\left(\chi - \beta\right)\ , \tag{6.11}
$$

where the χ_j have been given in (6.3), χ is given as

$$
\chi(x,t) = kx - \omega t \tag{6.12}
$$

and

$$
k = \frac{k_1 + k_2}{2} \quad \text{and} \quad \omega = \frac{\omega_1 + \omega_2}{2}\ . \tag{6.13}
$$

This signal may be written as

$$
\zeta(x,t) = a(x,t)\cos\left(\chi - \beta\right)\ , \tag{6.14}
$$

where a and β are given by

$$
\begin{aligned}
a^2 &= a_1^2 + a_2^2 + 2a_1a_2\cos\left(\Omega_1 - \Omega_2\right) \\
\tan\beta &= -\frac{a_1\sin\Omega_1 + a_2\sin\Omega_2}{a_1\cos\Omega_1 + a_2\cos\Omega_2}
\end{aligned}
\tag{6.15}
$$

with

$$\Omega_1 = \chi_1 - \chi \quad \text{and} \quad \Omega_2 = \chi_2 - \chi \tag{6.16}$$

so that

$$\Omega_1 - \Omega_2 = (k_1 - k_2)\,x - (\omega_1 - \omega_2)\,t + \vartheta_1 - \vartheta_2\ . \tag{6.17}$$

The variation in x of the squared amplitude a^2 occurs with $\cos[(k_1 - k_2)\,x]$ so that the variation in a occurs with $\cos\left(\frac{1}{2}(k_1 - k_2)\right)$ and the group length L_g is thus[2]

$$L_g = \frac{\pi}{|k_1 - k_2|}\ . \tag{6.18}$$

For the tapering we should thus have preferably

$$(x_r - x_\ell) > L_g = \frac{\pi}{|k_1 - k_2|}\ . \tag{6.19}$$

It should be stressed that it is not necessary to apply the tapering over one wave group, we also could have a number of groups and the tapering applied only at the outside groups. However, it should be realised that the initial wave profile should fit as a whole on a horizontal part of the bottom. With a long initial profile the computation necessarily takes more computer time in order to be able to see the same features of evolution of the waves. The computational domain is necessarily larger.

6.3.3 Example of input file

An example of an input-file for perphi (for the case p3) is given below.

```
#
# Inputfile voor berekeningen perphi
#
# Time parameters : dt , Nt , Ntwrt     (1 real,2 integers)
#
.1  500  5
#Depth foreland (m) , Depth bar (m)   , Depth hinterland (3 positive reals)
0.50 0.25  0.25
#Slope     1st       ,  2nd slope      , (2 reals , uphill = + , downhill = - )
#
.05  0.
#Width foreland (m) , Width bar (m)    , Width hinterland (m) (format : 3 reals)
60.  60.  0.0
#  gravity
  9.81
#  no. of components
```

[2] A simplification is obtained for equal phase shifts, $\vartheta_1 = \vartheta_2$; then $\Omega_1 = -\Omega_2$ and for $\tan\beta$ is obtained $\tan\beta = \frac{a_2 - a_1}{a_1 + a_2}\tan\Omega_1$. A further simplification is obtained when the amplitudes are equal, $a_1 = a_2$. Then $\beta = 0$ and $a^2(x,t) = 2a_1^2[1 + \cos(\Omega_1 - \Omega_2)] = 4a_1^2\cos^2\left\{\frac{1}{2}(\Omega_1 - \Omega_2)\right\}$, and thus, $a(x,t) = 2a_1\cos\left(\frac{1}{2}(k_1 - k_2)\,x - \frac{1}{2}(\omega_1 - \omega_2)\,t\right)$.

```
2
#  frequencies (in Hz)
0.48    0.39
#  amplitude (dimensional, in m)
0.054   0.012
#  phases (rad.)
0.0     0.0
#  interval (dim) for damping: xL and xr,  and x0
8.0     32.0    20.
#  rate(6/[L_d]) of damping
0.4     0.4
#  dx (in m)
0.6
#Aantal uitvoerstations (max 6)
6
#Plaatsen (in m)
30.0  40.0  65.0  80.0  95.0  110.0
```

7 Numerical examples

Some numerical examples will be discussed in this chapter. Both the time-domain model, **hamilT** and the sinc-based spectral model **sinctm** are used. The numerical examples are carried out either to show the possibilities of the programs or to estimate the accuracy of the computations. The problems considered in the present chapter correspond to non-breaking waves leaving the comments on breaking waves to the next chapter.

7.1 Solitary waves

To meet the purposes stated above we start with computing the evolution of a solitary wave over a horizontal bottom. With the help of the program **solphi** a free surface elevation $\zeta(x)$ and the corresponding free surface velocity potential $\varphi(x)$ are computed, given the height of the wave. The profile so computed is the exact solitary wave profile determined according to a method by Tanaka (1986). In fact, a modification of Tanaka's program has been used. Presently the inversion of a matrix has been carried out using a routine from the NAG library, which is available for MSDOS. It is the objective to use another routine (*e.g.*, from Numerical Recipes, see Press et al., 1992) so that the program becomes portable.

A single solitary wave

As Tanaka's profile gives the exact solitary wave solution, and our formulation is an approximate one, the initial solitary wave profile is not expected to remain conserved upon propagation. The computed example with $H/h = 0.4$ and $h = 10$ m shows what kind of oscillatory tail develops. The computed profiles at time $t = 0$, $t = 30$ and $t = 60$ s are shown in Figure 7.1 for **hamilT** and in Figure 7.2 for **sinctm**. These computations are performed with $\varepsilon = 0$ and the ABM integration method has been used. Figure 7.3 shows that the results with both programs are indeed identically.

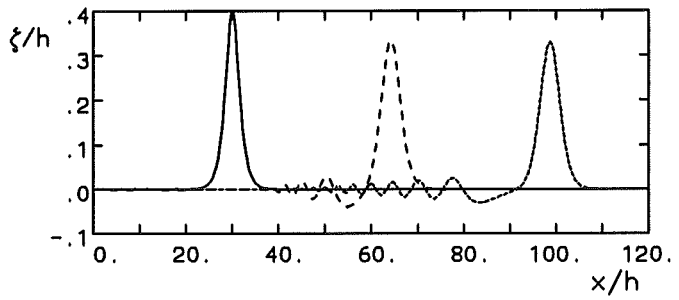

Figure 7.1: Solitary wave with $H/h = 0.4$, $h = 10$ m, hamilT; $t = 0$, 30 and 60 s.

As the inclusion of some more nonlinear terms is possible in the programs, the parameter icleps has been set equal to 2 so that is taken for B_1 the expression $B_1 =$

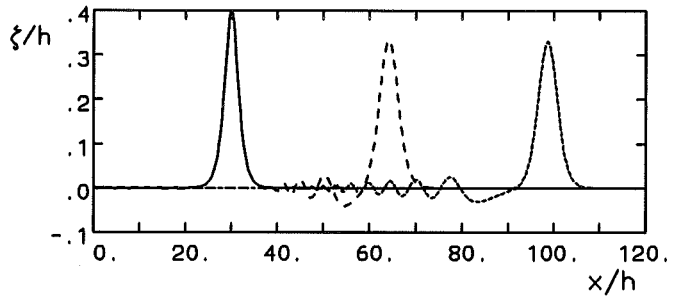

Figure 7.2: Solitary wave with $H/h = 0.4$, $h = 10\,\mathrm{m}$, sinctm; $t = 0$, 30 and 60 s.

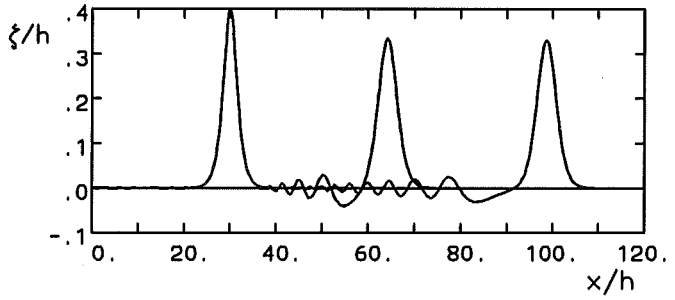

Figure 7.3: Solitary wave with $H/h = 0.4$, $h = 10\,\mathrm{m}$, for both hamilT and sinctm; $t = 0$, 30 and 60 s.

$1/\left[(1+\varepsilon)\eta^2\right]$ and the expression for ε follows from (2.51). The result is given in Figure 7.4. The difference with the case $\varepsilon = 0$ is only very slight. That the case icleps $= 1$ in which ε is given by (2.51) and B_1 follows from the full expression (2.50) leads to rapid development of instabilities is seen in Figure 7.5. Within 13 time steps of $\Delta t = 0.05\,\mathrm{s}$ the program stops.

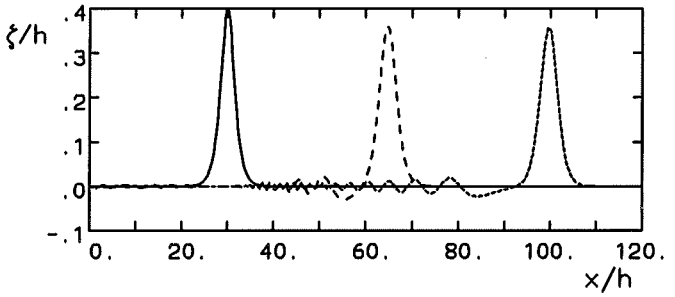

Figure 7.4: Solitary wave with $H/h = 0.4$, $h = 10\,\mathrm{m}$, nonlinearity according to icleps $= 2$, sinctm; $t = 0$, 30 and 60 s.

Two opposing solitary waves

The evolution of two solitary waves of equal height, but propagating in opposing direction in water of constant depth is shown in Figures 7.6 - 7.16. The individual wave height H/h is 0.3 with the depth $h = 10$ m, and $\Delta t = 0.1$ s and $\Delta x = 2$ m. The kinetic, potential and total energy are shown as function of time step in Figure 7.17. As could be expected beforehand, at the moment of total overlapping the resulting velo-

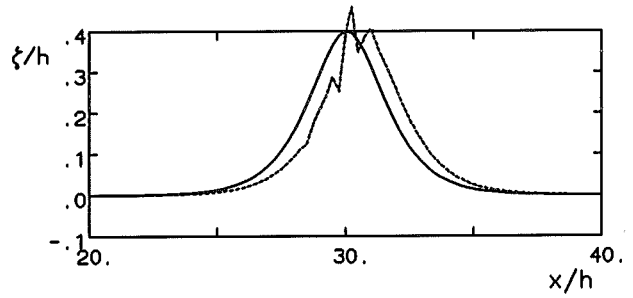

Figure 7.5: Solitary wave with $H/h = 0.4$, $h = 10\,\mathrm{m}$, nonlinearity according to icleps = 1, sinctm; $t = 0$ and 0.6 s

city equals zero and all energy is potential energy. The total energy remains constant, except for the last time steps when the solitary waves pass through the boundaries.

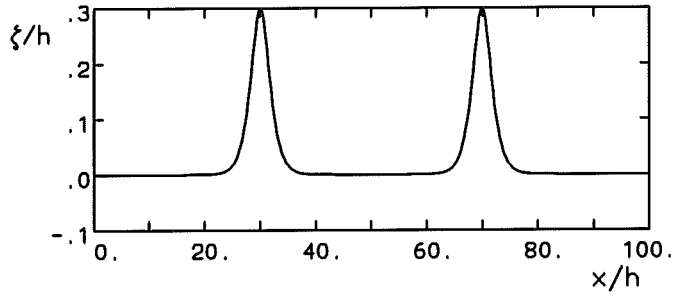

Figure 7.6: Two opposing solitary waves with $H/h = 0.3$, $h = 10\,\mathrm{m}$, nonlinearity according to icleps = 2, hamilT, $t = 0$ s

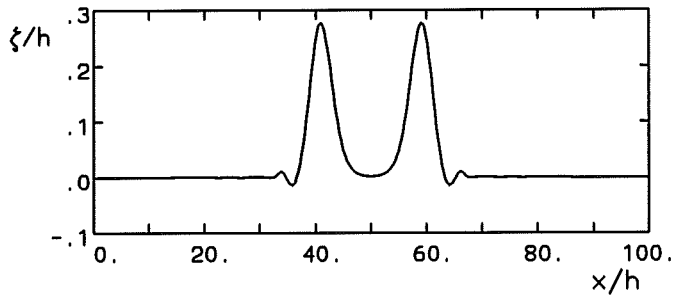

Figure 7.7: Two opposing solitary waves with $H/h = 0.3$, $h = 10\,\mathrm{m}$, nonlinearity according to icleps = 2, hamilT, $t = 10$ s

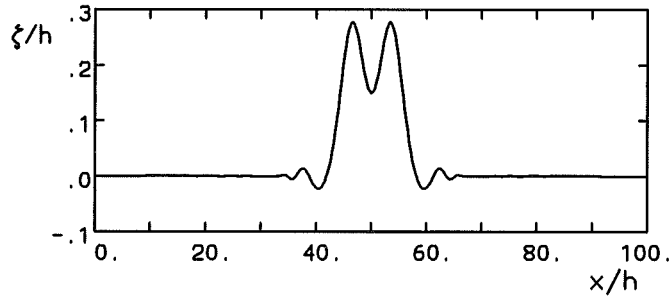

Figure 7.8: Two opposing solitary waves with $H/h = 0.3$, $h = 10\,\mathrm{m}$, nonlinearity according to icleps = 2, hamilT, $t = 15$ s

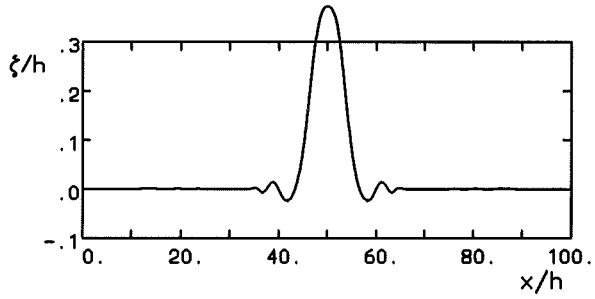

Figure 7.9: Two opposing solitary waves with $H/h = 0.3$, $h = 10\,\mathrm{m}$, nonlinearity according to icleps = 2, hamilT, $t = 16.5$ s

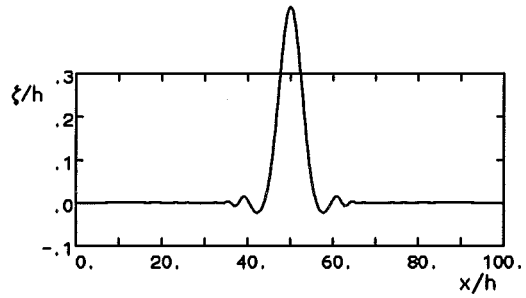

Figure 7.10: Two opposing solitary waves with $H/h = 0.3$, $h = 10\,\mathrm{m}$, nonlinearity according to icleps = 2, hamilT, $t = 17$ s

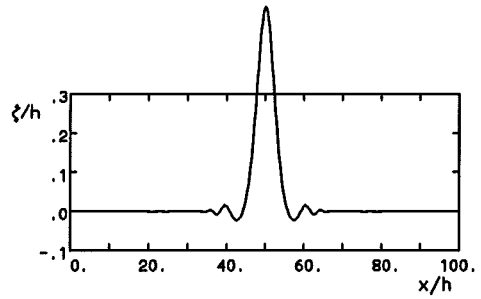

Figure 7.11: Two opposing solitary waves with $H/h = 0.3$, $h = 10\,\mathrm{m}$, nonlinearity according to icleps = 2, hamilT, $t = 17.5$ s

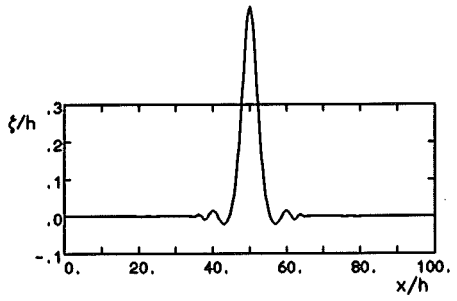

Figure 7.12: Two opposing solitary waves with $H/h = 0.3$, $h = 10\,\mathrm{m}$, nonlinearity according to icleps = 2, hamilT, $t = 18$ s

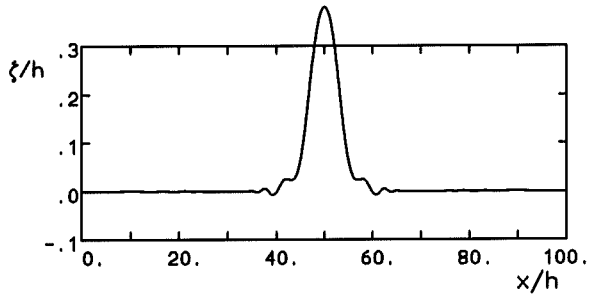

Figure 7.13: Two opposing solitary waves with $H/h = 0.3$, $h = 10\,\mathrm{m}$, nonlinearity according to icleps = 2, hamilT, time = 20 s

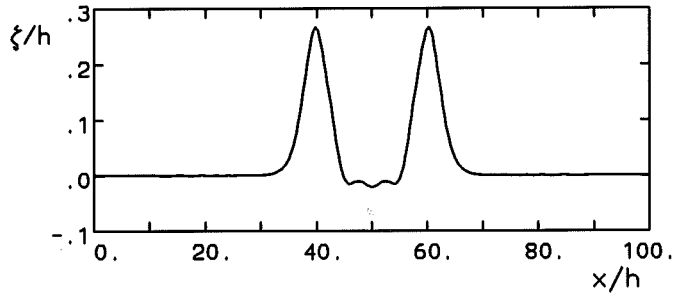

Figure 7.14: Two opposing solitary waves with $H/h = 0.3$, $h = 10\,\mathrm{m}$, nonlinearity according to icleps = 2, hamilT, $t = 27.5$ s

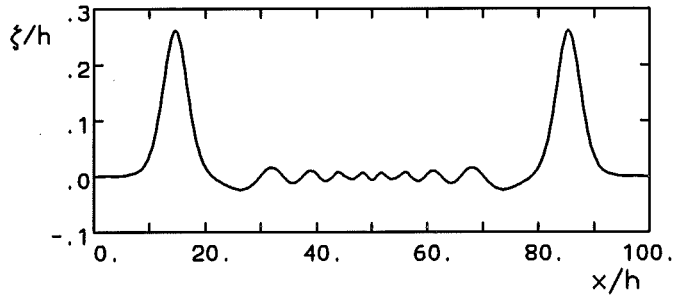

Figure 7.15: Two opposing solitary waves with $H/h = 0.3$, $h = 10\,\mathrm{m}$, nonlinearity according to icleps = 2, hamilT, $t = 50$ s

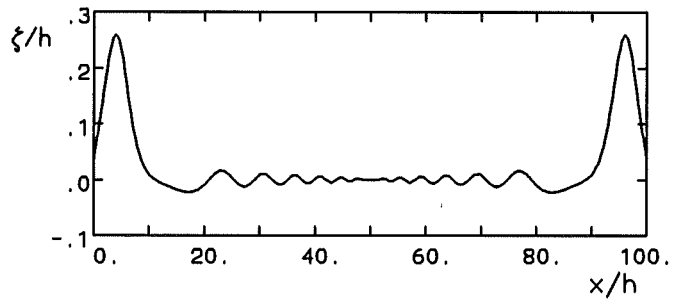

Figure 7.16: Two opposing solitary waves with $H/h = 0.3$, $h = 10\,\mathrm{m}$, nonlinearity according to icleps = 2, hamilT, $t = 59.5$ s

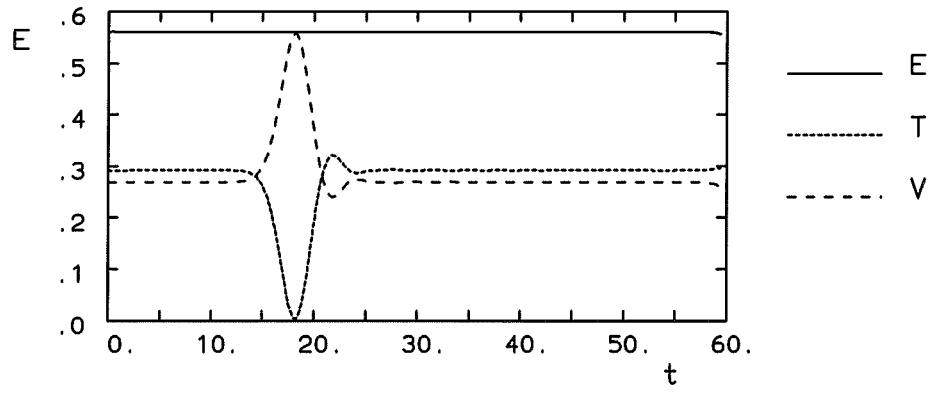

Figure 7.17: Two opposing solitary waves with $H/h = 0.3$, $h = 10\,\mathrm{m}$, nonlinearity according to icleps = 2, hamilT, kinetic, potential and total energy as function of time step

7.2 Periodic waves

As we have an initial value problem, at most a finite wave train is permitted. The whole of the wave train has to be contained in the computational domain at time $t = 0$.

Wave group

We fist give some results of the progress of a (linear) wave group on a shelf-like bottom geometry. We show results of computation p3, of which the input has been given in section 6.3.3. A biharmonic signal is considered with frequencies 0.39 and 0.48 Hz and amplitudes of 1.2 cm and 5.4 cm. As we need zeroes at both ends the artificial damping method has been applied. In this way we get an initial wave profile as shown in Figure 7.18. Notice that because this is a linear wave group we have symmetry around $z = 0$. Upon evolution with the nonlinear model (with $\varepsilon = 0$), a recurrent behaviour is seen to occur (Figs. 7.19 - 7.22), as is also the case with, *e.g.*, Boussinesq-type of programs in which a sinusoidal wave profile at the boundary is used. On the shelf larger nonlinear behaviour is seen to develop, see Figures 7.23 - 7.26 for the time steps 750, 1125, 1200 and 2175.

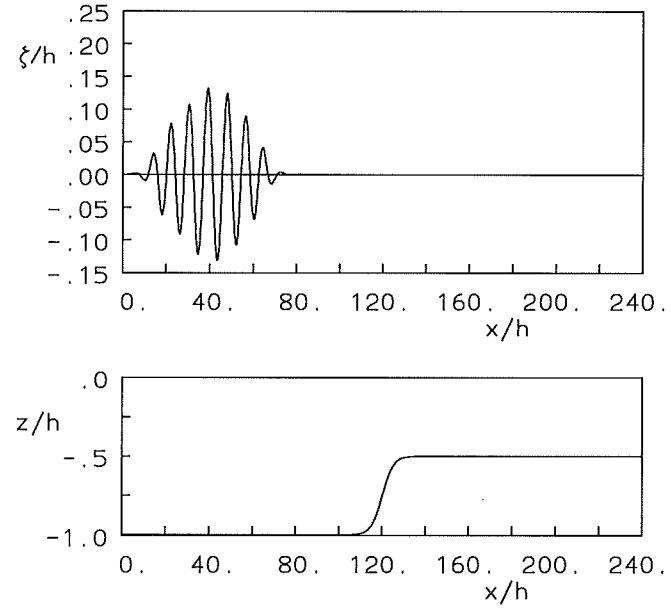

Figure 7.18: Wave group p3, $t = 0$

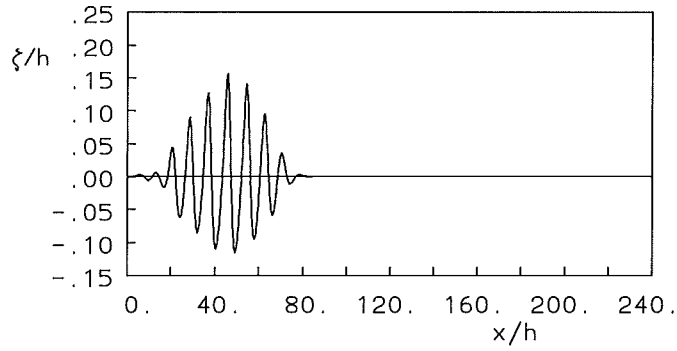

Figure 7.19: Wave group p3, $t = 75\Delta t$

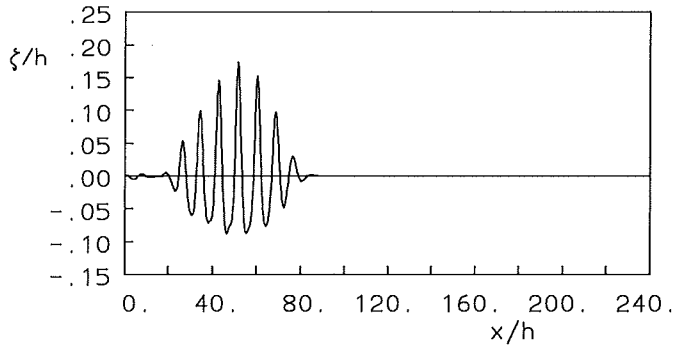

Figure 7.20: Wave group p3, $t = 150\Delta t$

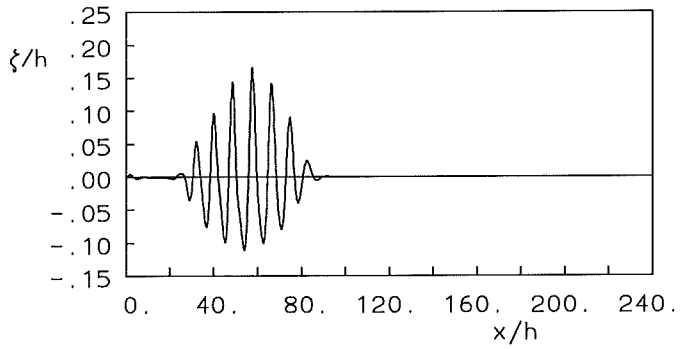

Figure 7.21: Wave group p3, $t = 225\Delta t$

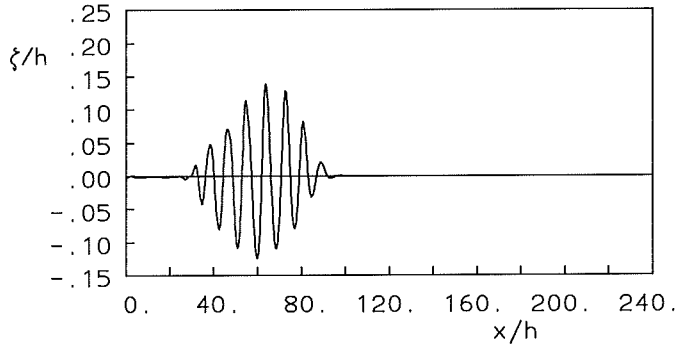

Figure 7.22: Wave group p3, $t = 300\Delta t$

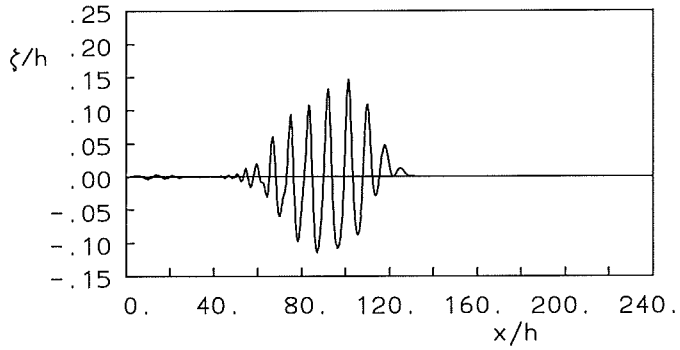

Figure 7.23: Wave group p3, $t = 750\Delta t$

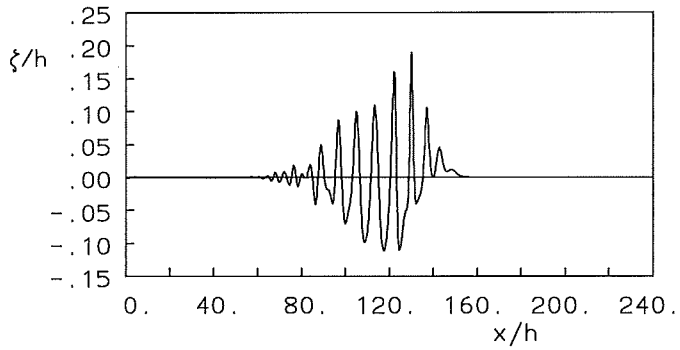

Figure 7.24: Wave group p3, $t = 1125\Delta t$

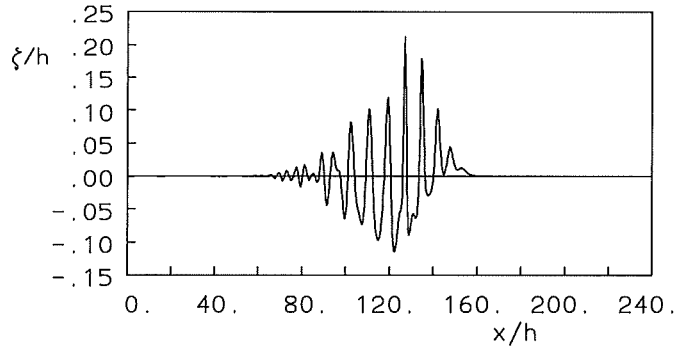

Figure 7.25: Wave group p3, $t = 1200\Delta t$

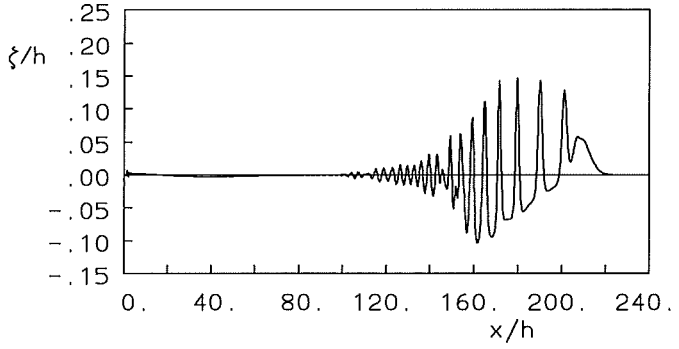

Figure 7.26: Wave group p3, $t = 2175\Delta t$

7.3 Confrontation with measurements

The Hamiltonian model has been applied to the problem of wave propagation over an underwater bar. The bottom geometry and the location of the wave gages are indicated in Figure 7.27.

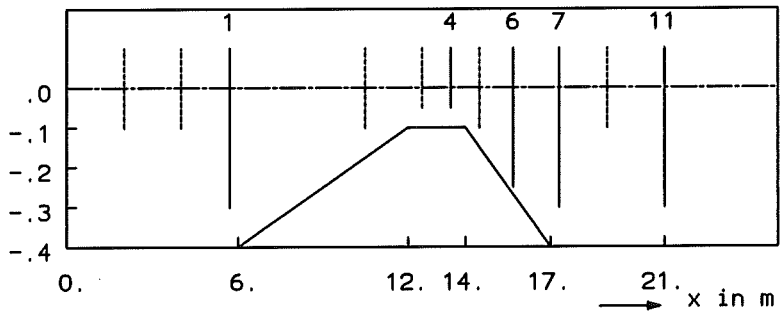

Figure 7.27: The bottom geometry and the location of the wave gauges.

In this case the incoming wave consists of a sinusoidal wave with wave height $H = 1$ cm and wave period $T = 2.02$ s. This is one of the cases measured by Battjes and Beji (1993), and repeated on a linear scale of 0.5 (i.e., the initial depth equals 80 cm instead of 40 cm) by Klopman. The measurements of Klopman are used because of the active wave absorption and the compensation of bound long waves; two important processes which have not been accounted for in the measurements of Battjes and Beji. A further description of the measurements is given in Dingemans (1994a). Here we consider the measurement condition A.

It is not possible at the moment to let waves enter the region through the left-hand boundary (a so-called boundary value problem) in the numerical Hamiltonian model. Only the treatment of initial value problems are possible. Therefore we have to impose a wave train and to be able to do so we have to extend the initial horizontal bottom region leftwards. A train of sinusoidal waves is used, where at the front and the end of the train the free surface elevation goes to zero smoothly. The specification of the initial condition goes in the same way as before. For the numerical example shown here the initial wave packet is a monochromatic signal, consisting of seventeen waves (fig. 7.28). From the time records of elevation at the locations of the wave gauges we take the midportion of the signal for comparison with the measurements. Computed (Hamiltonian, with $\varepsilon = 0$), measured and computed (exact nonlinear) elevations are shown in Figure 7.29 over a few wave periods.

In order to show the performance more clearly, we also plot the computed and measured free surface profiles at 21 m together. This is done in Figure 7.30 for the Hamiltonian model and for the boundary element program Hypan.

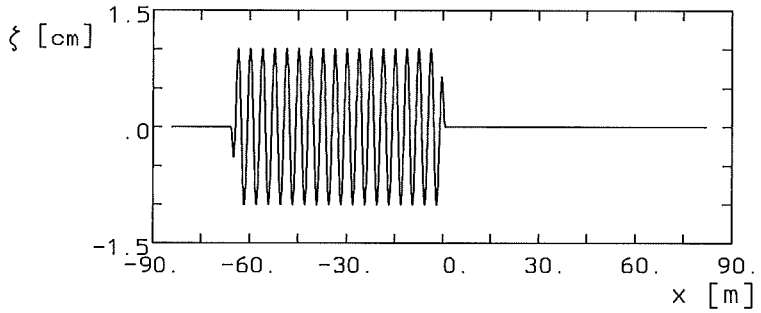

Figure 7.28: The initial value $\zeta(x, 0)$.

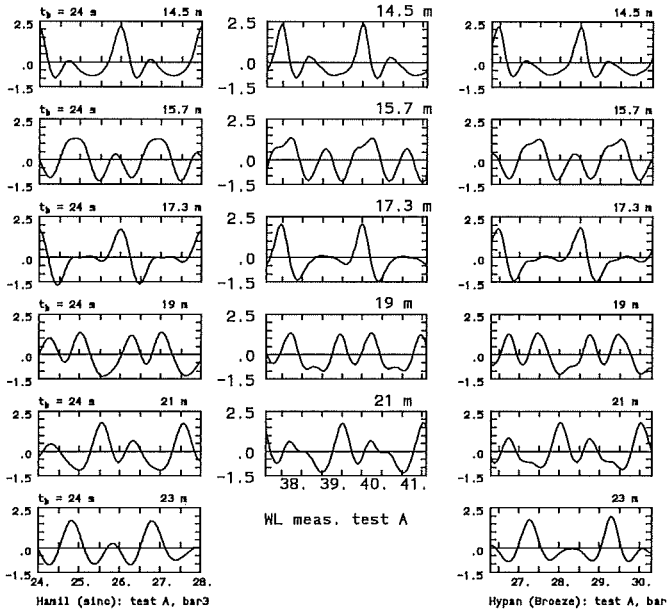

Figure 7.29: A Hamiltonian model (left), measurements (middle) and the Hypan model of Broeze (right), test A.

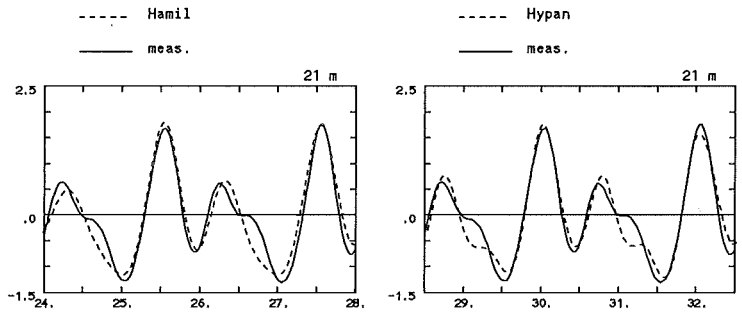

Figure 7.30: Comparison of the Hamiltonian model (left) and the Boundary-Element model (right) with the measurement at 21 m.

8 Modelling of breaking

In this chapter we consider extending the Hamiltonian model of wave propagation for breaking waves. This amounts to simulating the effects of breaking in a model which is strictly valid for nonbreaking waves. The motivations behind this are twofold: the model can then be used from offshore to onshore without problems of numerical instabilities if wave breaking should occur; secondly, as many breaking-related phenomena (for example, decay in wave energy, set-up of mean water level) as possible can in some realistic way be simulated through the model. Since the evolution equations are approximate, the physical phenomenon of breaking may manifest in the form of other mechanisms in the mathematical model. Two primary aspects of the simulation of breaking are therefore a criterion for wave-breaking and secondly, a model for adjusting the surface variables near the breaking region. From the point of the first motivation alone, mathematical behaviour of the evolution equations in situations where waves do physically break need to be investigated. In fact, this aspect may necessitate that the breaking criterion to be imposed is model-specific.

8.1 Criterion for breaking

The breaking criterion used here is based on the Jacobian of the transformation from the physical space to the χ-space. We assume breaking to occur if

$$\frac{d\chi}{dx} = 0. \tag{8.1}$$

An approximate integral expression of (8.1) is given by (Dingemans and Radder, 1991)

$$\eta(p) + \int_0^\infty \frac{dq}{\exp(\pi q) - 1} \frac{d}{dq} [\zeta(p+q) + \zeta(p-q)] = 0 \tag{8.2}$$

with

$$p(x') = \int_{-\infty}^{x'} \frac{dr}{\eta}; \quad q(x', r) = \int_{x'}^{x'+r} \frac{dr}{\eta} \quad (\text{for } r \geq 0) \tag{8.3}$$

The criterion (8.1) comes from the mathematical requirement that the transformation remains nonsingular and well-behaved. It has been subsequently shown by Radder (1993b) that (8.2) does indeed predict the critical steepness in a reasonable manner in several different situations; namely deep-water Stokes waves, solitary wave, an asymetric wave and standing waves.

Before applying the criterion (8.2) in the numerical scheme, the question of singular behaviour of the function $1/[\exp(\pi q) - 1]$ at $q = 0$ is first investigated. Secondly, a more amenable form of the expression is discussed in connection with the numerical scheme based on the physical space.

8.1.1 Behaviour of the integrand near $q = 0$

It follows through Taylor's expansion around $q = 0$ that

$$\zeta(p+q) + \zeta(p-q) = 2\zeta(p) + q^2 \frac{d^2\zeta}{dq^2}(p) + O(q^4) \tag{8.4}$$

and

$$\exp(\pi q) - 1 = \pi q + \frac{(\pi q)^2}{2} + \cdots \tag{8.5}$$

leading to

$$\frac{\frac{d}{dq}[\zeta(p+q) + \zeta(p-q)]}{\exp(\pi q) - 1} = \frac{2}{\pi\left(1 + \frac{\pi q}{2}\right)} \frac{d^2\zeta}{dq^2}(p) + O(q^2) \tag{8.6}$$

for small q.

8.1.2 Integral criterion in physical space

The breaking criterion (8.2) is not convenient for numerical evaluation since the evolution equations are computed on uniformly spaced grids in the physical space. In deriving an equivalent expression in the physical space special attention has to be paid to the behaviour of the integrand near $r = 0$. We proceed as follows.

$$\begin{aligned} \eta(p) + \int_0^\infty \frac{dq}{\exp(\pi q) - 1} \frac{d}{dq}[\zeta(p+q) + \zeta(p-q)] = \\ \eta(p) + \int_0^\infty \frac{dq}{\exp(\pi q) - 1} \left[\frac{d}{dq}\zeta(p+q) - \frac{d\zeta}{dq}(p)\right] + \\ \int_0^\infty \frac{dq'}{\exp(\pi q') - 1} \left[\frac{d}{dq'}\zeta(p-q') + \frac{d\zeta}{dq'}(p)\right] \end{aligned} \tag{8.7}$$

where

$$q(x,r) = \int_x^{x+r} \frac{dr}{\eta} \quad , \quad q'(x,r) = \int_x^{x-r} \frac{dr}{\eta} \, . \tag{8.8}$$

Note that each of the integrand in (8.7) near $q = 0$ is still well-behaved through the introduction of the term $d\zeta/dq(p)$. The breaking criterion in the physical space can then be written as

$$\begin{aligned} \eta(x) + \int_0^\infty \frac{dr}{\exp(\pi q) - 1} \left[\frac{d}{dr}\zeta(x+r) - \frac{\eta(x)}{\eta(x+r)} \frac{d\zeta}{dr}(x)\right] + \\ \int_0^\infty \frac{dr}{\exp(\pi q') - 1} \left[\frac{d}{dr}\zeta(x-r) + \frac{\eta(x)}{\eta(x-r)} \frac{d\zeta}{dr}(x)\right] = 0 \end{aligned} \tag{8.9}$$

Both the integrands in (8.9) have removable singularity at $r = 0$, *i.e.*,

$$\left.\frac{\frac{d}{dr}\zeta(x+r) - \frac{\eta(x)}{\eta(x+r)}\frac{d\zeta}{dr}(p)}{\exp(\pi q) - 1}\right|_{r=0} = \left.\frac{\frac{d}{dr}\zeta(x-r) + \frac{\eta(x)}{\eta(x-r)}\frac{d\zeta}{dr}(p)}{\exp(\pi q') - 1}\right|_{r=0}$$
$$= \frac{1}{\pi}\left[\eta\frac{d^2\zeta}{dr^2} + \left(\frac{d\zeta}{dr}\right)^2\right] . \tag{8.10}$$

Equivalent to the breaking criterion (8.9), a breaking index B_r, given by,

$$B_r(x) = -\frac{[\cdots]}{\eta(x)} \tag{8.11}$$

[with $[\cdots]$ denoting the values of the two integrals in (8.9)] may be defined requiring $B_r = 1$ as the criterion of breaking.

Since the maximum contribution to the integral in (8.11) comes from the value of the integrand near $r = 0$ (or $q = 0$), an interpretation of the breaking index is easily obtained from (8.10). The breaking criterion depends on both the slope and the curvature of the surface. Further, it is clear after dividing (8.10) by η [as in (8.11)] that the curvature is dominant in deeper water and slope becomes increasingly important on shallower water.

8.2 Modification of surface evolution

The surface elevation ζ is modified if the breaking index B_r exceeds the limiting value at a point x_b. Let the modified surface elevation be ζ'. The modification is based on two principles:

Breaking index The surface elevation ζ' is such that the maximum value of the breaking index at x_b calculated on the basis of ζ' is B_r^m, the allowable limit for B_r (mathematically 1).

Mass conservation The modified surface elevation does not lead to change in the mass; *i.e.*, the mass of water contained under the unmodified surface elevation is maintained.

From the first requirement of breaking index, ζ' must satisfy the equation

$$\int_0^\infty \frac{dr}{\exp(\pi q) - 1}\frac{d}{dq}\left[\zeta'(p+q) + \zeta'(p-q)\right] = -\eta'(x_b)B_r^m \tag{8.12}$$

with p and q defined on the basis of ζ' and from the second requirement of maintaining the mass the condition that

$$\int_{-\infty}^\infty \zeta' dx = \int_{-\infty}^\infty \zeta dx . \tag{8.13}$$

The two conditions given by (8.12) and (8.13) govern the way surface elevation should be modified at two grid points. We fix these two grid points to be the grid point where

the breaking index exceeds its limit and the next adjacent grid in the direction of wave propagation. A direct solution of the equations to solve for the modified surface elevation will be immensely time consuming and may be unnecessary since the values of elevation at only two grid points near x_b are modified. A local solution of (8.12) and (8.13) will therefore be adopted.

8.3 Modification of velocity evolution

Consider first an approach where the breaker front is stationary with respect to a reference frame moving at speed c_b. Following Banner and Phillips (1974) we impose that

$$\frac{\partial}{\partial s}\left(\frac{1}{2}u_s^2 + g\zeta'\right) = 0 \tag{8.14}$$

or, equivalently

$$\left(\frac{1}{2}u_s^2 + g\zeta'\right) = \text{const} \tag{8.15}$$

where u_s is the tangential velocity on the free surface with respect to the moving reference frame. Expressing (8.14) with respect to the fixed frame, we have

$$\frac{1}{2}\frac{(c_b - v')^2}{1 + \zeta_x'^2} + g\zeta' = \text{const} \tag{8.16}$$

The modified velocity v' can now be obtained through (8.16) using the modified surface elevation provided the speed c_b of the breaker front is known. An estimation in the form of $c_b = \alpha\sqrt{g\eta_b}$ with η_b as the local maximum of η near the breaking point and α as a constant coefficient is likely to be less than satisfactory. This is due to the question about both the right value of the speed c_b and the validity of (8.15).

An alternative approach suggested by Radder is to modify the velocity through an estimation of the energy lost to the rotational field. The approach is as follows. The exact kinematic condition on the free surface, for irrotational and rotational field as well, gives

$$\frac{\partial\zeta}{\partial t} = \frac{ds}{dx}v_n \tag{8.17}$$

where v_n is the velocity normal to the surface. Let Δv_n represent the induced rotational velocity due to the process of breaking. The rotational velocity Δv_n is then related to the change in surface elevation so as to satisfy the kinematic free surface condition (8.17) on the modified surface,*i.e.*,

$$\Delta\zeta_t = \frac{\partial\zeta'}{\partial t} - \frac{\partial\zeta}{\partial t} = \frac{ds}{dx}(\Delta v_n)\,.$$

Expressing the rotational kinetic energy density T_r to be $T_r = 0.5(\Delta v_n)^2$, modification of the surface velocity is governed by the principle that

$$T' = T - T_r \tag{8.18}$$

where T is the unaltered kinetic energy density, given by,

$$T = \frac{1}{2}\left(v_s^2 + v_n^2\right) = \frac{1}{2}\left(\frac{dx}{ds}\right)^2 (v^2 + \zeta_t^2). \tag{8.19}$$

Assuming that ds/dx remains constant, we have from (8.18)

$$(v'^2 + \zeta_t'^2) = (v^2 + \zeta_t^2) - (\Delta\zeta_t)^2$$

leading to the relation

$$v'^2 = v^2 - 2\zeta_t'\Delta\zeta_t \tag{8.20}$$

Expression (8.20) is the basis for computing the modified velocity v' at the grid points where the surface elevation is modified.

We note from previous discussion of modification of mass flux that the change in ζ is positive at one of the points and negative at the other. This has the consequence that the magnitude of the modified velocity is decreased at one point (the point where $\Delta\zeta$ is positive) and increased at the other as can be seen from (8.20).

8.4 Study of breaking criterion

The breaking index in the numerical code is evaluated according to the formulation (8.11) with the value of the integrand at $r = 0$ being determined from (8.10). In the following, we present a few numerical examples of the computation of the breaking index.

8.4.1 Verification of computation of breaking index

First, a few examples are selected so that the computation of the breaking index can be compared against analytical solutions.

The first case studied is that of a Stokes fifth-order wave in deep water. The breaking index obtained from analytical evaluation of (8.11) for a surface form given by

$$\zeta = \sum_{l=1}^{n} a_l \cos lkx \tag{8.21}$$

is (Radder, 1993b)

$$B_r = \sum_{l=1}^{n} lka_l \cos lkx \tag{8.22}$$

for the limiting case of infinite depth. The value of $ka_l = 0.458$ leads to a breaking index of 1 at the crest of the waves. Breaking index as computed numerically over different depths and that as computed for the limiting case of infinitely deep water from (8.22) are shown in Fig. 8.1 where the coefficients a_l's are assumed according to Stokes fifth-order waves in deep water. In the numerical examples, a train of waves with leading and trailing edges are considered while the wave train in the analytical solution is infinitely uniform. The maximum value of the computed breaking index is lower than 1, though it tends toward 1 with increasing depth. One of the reasons for the difference between the computed and the analytical values is that the shown computed values are for specific depths while the analytical values are for infinitely deep water.

Computed and analytical breaking index for a train of asymmetric waves are shown in Fig. 8.2. The surface elevation is assumed to be of the form (up to two terms):

$$\zeta(x) = a\left[-\sin kx - \frac{1}{2^2}\sin 2kx\right] . \tag{8.23}$$

and the corresponding analytical breaking index (Radder, 1993b) is given by

$$B_r(x) = -ka\left[\sin kx + \frac{1}{2}\sin 2kx\right] . \tag{8.24}$$

The computed values are again somewhat different from the analytical values, though the differences may be due to the finite depth used in the computation.

8.4.2 Breaking index for waves over a bar

For the specific purpose of waves breaking during propagation due to variation in depth, we consider a train of waves propagating on to a bar similar to the situation in the experimental setup of Luth *et al.* (1994). For the case presented in Fig. 8.3, wave period is 2.5254 s and the incident wave height H_i is 0.0279 m over an uniform depth of 0.4 m. These conditions were observed to generate a spilling breaker over the bar in the experiment.

To check if breaking is predicted in the numerical model maximum value of the breaking index $B_r(x)$ as computed from (8.11) and its location x are recorded at each time step. These maximum values and the spatial coordinates of their occurrences are shown in Fig. 8.3. The maximum value of the computed breaking index is around 0.2, far too low to indicate any breaking.

In order to gain some insight into the rather low value of the breaking index in the numerical computation, a comparison of the measured and numerical surface elevation

is shown in Figs. 8.4 and 8.5. The measured elevation at $x = 12.5$ m (Fig. 8.4) and $x = 13.5$ m (Fig. 8.5) show much sharper and higher peak than the computed time record though the computed peaks are higher than the measured peaks at the stations on the back-slope of the bar. In the experiment spilling breakers were observed in the region from 13.5 m to 15 m. It is seen clearly that the high crest value before the breaking region is underpredicted in the numerical model. The height of the measured wave is subsequently lower than the numerical values on the back slope of the bar due to the energy loss due to breaking. The comparison indicates that the model prediction of the sharp, high value of the crest is unsatisfactory (possibly due to the absence of the short-wave nonlinearity from the formulation).

8.5 Summary

Based on the computed results presented in Figs. 8.3, 8.4 and 8.5 the low value of the breaking index can be attributed to the model (under)prediction of sharper, higher crests since the breaking criterion (8.11) is found to be reasonable (see Fig. 8.1) provided the surface form has the right curvature and slope. It is believed that the short-wave nonlinearity ε has a significant contribution to the surface form near the crest. Though the inclusion of the short-wave nonlinearity as described in chapter 6 led to unstable computations, partial (ad-hoc) nonlinearity (**icleps**=2) has been found to give better results during the propagation of a solitary wave. An important step in the future developments of the model should therefore be a stable formulation/implementation of the short-wave nonlinearity.

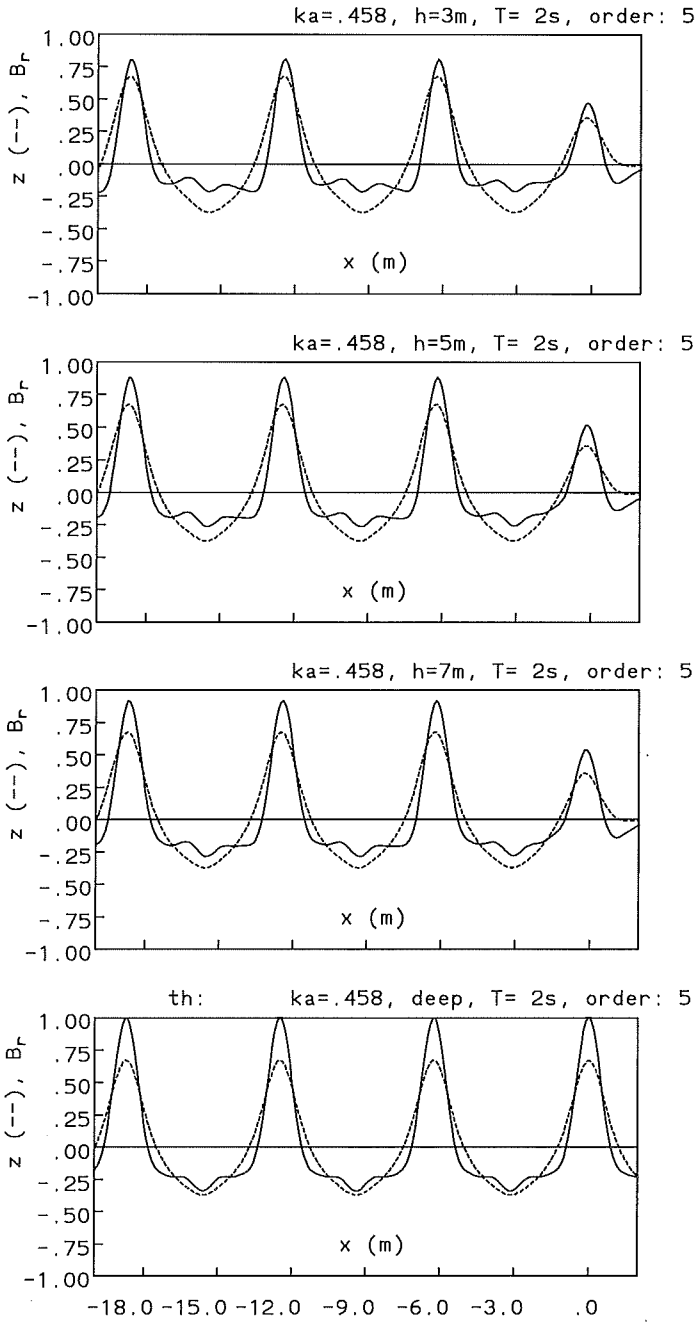

Figure 8.1: Computed (top three) and analytical (bottom) breaking index for a surface form given by (8.21) where the coefficients a_l's are specified according to Stokes fifth order waves in deep water.

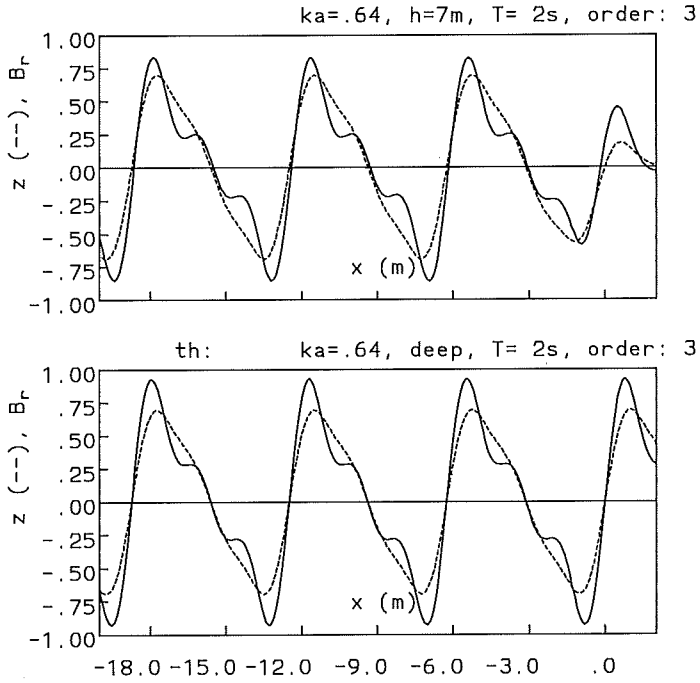

Figure 8.2: Computed (top) and analytical (bottom) breaking index for an asymmetrical surface form, given by (8.23), for $ka = 0.64$.

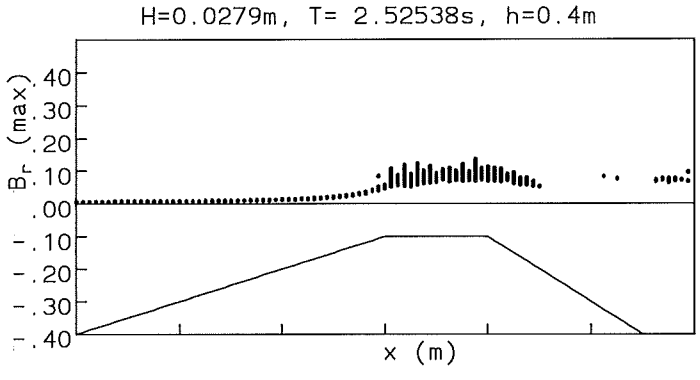

Figure 8.3: Maximum value of the breaking index and its spatial occurrence at each time step of computation. Breaking index is nondimensional while depth of the bar is plotted in units of meters.

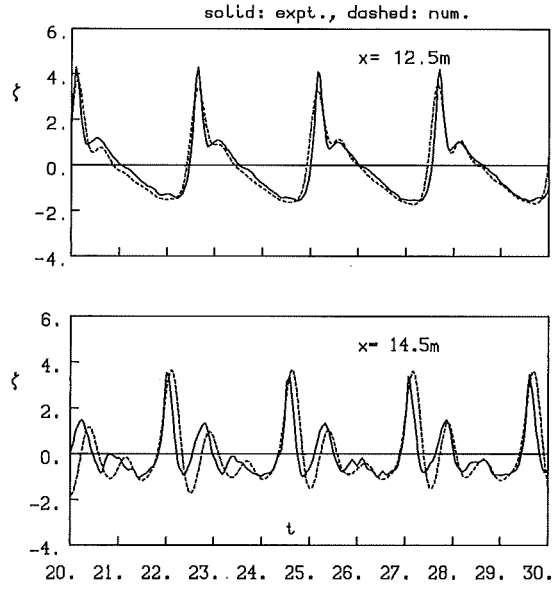

Figure 8.4: Time record of surface elevation from experimental measurement and numerical prediction. The time origin of the experimental measurement is shifted to roughly match the numerical record for the station at 12.5 m.

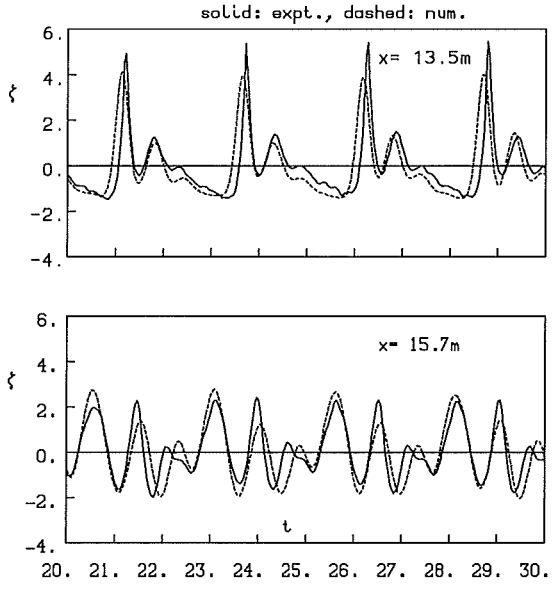

Figure 8.5: Time record of surface elevation from experimental measurement and numerical prediction. The time origin of the experimental measurement is shifted to roughly match the numerical record for the station at 13.5 m.

9 Conclusions

Two numerical models, '**hamilT**' and '**sinctm**' have been developed based on the approximate Hamiltonian, given by (2.17). Applications of these models to problems of both solitary and periodic waves over varying depth show their applicability as tools for modelling nonlinear wave transformation and interactions. A much larger time-step can be used by adopting ABM method of time integration instead of the first order, explicit Euler integration method without losing accuracy. The model '**sinctm**' based on the sinc approximation requires less computing time than the time-domain model '**hamilT**'.

One of the advantages of the formulation used here is the exact dispersion relationship exhibited in the linearised form. Secondly, the structure of the present approximate Hamiltonian allows developing the model formulation to be uniformly valid from deep to shallow water. From applications of the numerical model with the parameter **icleps**= 0 in chapters 7 and 8, it is seen that wave transformation and generation of higher harmonics are reasonably predicted for moderately long waves. It is believed further that even for moderately long waves short-wave nonlinearity plays an important role at least near regions of sharp crest and more so for higher waves. The formulation of short-wave nonlinearity through the function ε as described in chapter 2 (specified through the parameter icleps=1) has not been successful due to quick growth of instabilities. Ad-hoc inclusion of the positive definite part of ε (specified by the parameter icleps=2) indicates improvement in the model performance as shown through the propagation of a solitary wave. However, a complete and consistent procedure of including short-wave nonlinearity is still lacking. Extending the model formulation to include short-wave nonlinearity should therefore be one of the most important tasks in the future. This step is also necessary before further investigation into including effects of wave breaking can be carried out through this model.

As pointed out earlier, the formulations used here are derived on the basis of mildly-sloping bottom. This assumption can possibly be relaxed to account for steeper variation of the bottom along with a procedure to include short-wave nonlinearity. Then also the depth-dependent part in the function $x(\chi)$ has to be accounted for, see (2.12).

As the problem now solved is an initial-value problem, application of the model to problems of periodic waves is now carried out by an initial specification of a wave packet in front of the region of interest. This is computationally inefficient for problems of practical applications. More importantly, there is no clear procedure at the moment to translate input to the program in the form of a time-series of surface elevation or velocity as measured or recorded at a point to an $x-$series. It is desirable from this aspect to introduce procedures to effectively simulate generation and radiation boundaries. An associated problem is the numerical instabilities arising at the ends. Numerical instabilities begin to develop as the waves reach the boundaries of the computational domain. These instabilities may be reduced by a careful numerical treatment at the ends. Alternatively, this problem may be looked at in a consistent way along with the task of simulating generation and radiation boundary conditions.

Finally, application of the model to breaking waves shows that the computed breaking index with the assumption of $\varepsilon = 0$ is much lower than expected. The breaking criterion used has been found to be reasonable provided the shape and height of the surface corresponds to that of breaking. The low value of the computed breaking index is therefore attributed to model underprediction of crest height and sharpness before breaking. It is believed that this feature may be significantly improved by including short-wave nonlinearity.

Recommendations

A recapitulation of various points of further research is given below. The points are mentioned in order of importance for engineering applications.

1. The formulation of a boundary-value problem instead of an initial-value problem. This greatly enhances the practical usefulness of the program.
2. Inclusion of short-wave nonlinearity. For applicability over the full range of deep to shallow water of a nonlinear wave model, inclusion of short-wave nonlinearity is needed. Furthermore, it has been shown that for wave breaking also the inclusion of short-wave nonlinearity is needed to obtain more realistic breaker indices. A different formulation of $\varepsilon(x)$ in free surface quantities is needed because the present formulation leads to instability.
3. Further study of wave breaking characteristics after inclusion of short-wave nonlinearity.
4. Effect of steeper bottom slopes on the wave behaviour. The influence of the depth-dependent terms on $x(\chi)$ in (2.12) has to be accounted for then.

Bibliography

Banner, M.L. and O.M. Phillips (1974). On the incipient breaking of small scale waves. *J. Fluid Mechanics* **65**, pp. 647-656.

Beji, S. and J.A. Battjes (1993). Experimental investigations of wave propagations over a bar, *Coastal Engineering* **19(1,2)**, pp. 151-162.

Broer, L.J.F. (1974) On the Hamiltonian theory of surface waves. *Appl. Sci. Res.* **30**, pp. 430-446.

Dingemans, M.W. (1994a). Comparison of computations with Boussinesq-like models and laboratory measurements, MAST-G8, H1684, Delft Hydraulics.

Dingemans, M.W. (1994b). *Water Wave Propagation Over Uneven Bottoms.* World Scientific, Singapore, to be published.

Dingemans, M.W. and A.C. Radder (1991). Use of Hamiltonian techniques in water wave propagation problems, *Nonlinear Water Wave Workshop*, Ed. D.H. Peregrine, University of Bristol, pp. 24-31.

Dingemans, M.W., H.A.H. Petit, Th.J.G.P. Meijer, and J.K. Kostense, (1991). Numerical evaluation of the third-order evolution equations for weakly nonlinear water waves propagating over uneven bottoms. In: *Computer Modelling in Ocean Engineering 91*, Eds. A.S. Arcilla, M. Pastor, O.C. Zienkiewicz and B.A. Schrefler, Balkema, Rotterdam, pp. 361-370.

Dold, J. W. and Peregrine, D. H. (1986). An efficient boundary-integral method for steep unsteady water waves, in *Numerical Methods for Fluid Dynamics II*, eds. K. W. Morton and M. J. Baines. 671-679.

Greenberg, M. (1978). *Foundations of Applied Mathematics.* Prentice-Hall, New York.

Longuet-Higgins, M. S. and Cokelet, E. D. (1976). The deformation of steep surface waves on water. *Proc. R. Soc. Lond.*, **A350**, pp. 1-26.

Lund, J. and K.L. Bowers (1992). *Sinc Methods for Quadrature and Differential Equations*, SIAM, Philadelphi, 304 pp.

Luth, H.R, Klopman, G. and Kitou, N., 1994. Project 13G: Kinematics of waves breaking partially on an offshore bar; LDV measurements for waves with and without a net onshore current. *Delft Hydraulics* Report H1573, March 1994, 40 pp.

Otta, A.K. (1992). *Unsteady Free Surface Waves in a Region of Arbitrary Shape*, Ph.D dissertation, University of Delaware, Newark, Delaware.

Press, W.H., Teukolsky, S.A., Vettering, W.T. and Flannery, B.P. (1992). *Numerical Recipes in Fortran; The Art of Scientific Computing.* Second Edition. Cambridge University Press, 963 pp.

Radder, A. C. (1992). An explicit Hamiltonian formulation of surface waves in water of finite depth. *J. Fluid Mech.* **237**, pp. 435-455.

Radder, A.C. (1993a). A spectral Hamiltonian wave model based on the sinc method, Personal Note.

Radder, A,C. (1993b). An integral criterion for waves breaking in deep and shallow water, *Personal Note.*

Tanaka, M. (1986). The stability of solitary waves. *Physics of Fluids* **29**, pp. 650-655.

Woods, L. C. (1961). *The Theory of Subsonic Plane Flow.* Cambridge University Press, London.

Zakharov, V.E. (1968). Stability of periodic waves of finite amplitude on the surface of a deep fluid. *Zh. Prikl. Mekh. i Techn. Fiz.* **9(2)**, pp. 86-94 [*Soviet Physics, J. Appl. Mech. Techn. Phys.* **2**, pp. 190-194.]

Zienkiewicz, O. C. and K. Morgan (1983). *Finite Elements and Approximation*, John Wiley and Sons, New York.

Zwartkruis, T. J. G. (1991). Computation of solitary wave profiles described by a Hamiltonian model for surface waves. *Final Report of the Post-Graduate Programme*, Technische Universiteit Eindhoven, Eindhoven.